Study of In$_2$S$_3$ and ZnS thin films deposited by ultrasonic spray pyrolysis and chemical deposition

KAIA ERNITS

TALLINN UNIVERSITY OF TECHNOLOGY
Faculty of Chemistry and Materials Technology
Department of Materials Science
Chair of Semiconductor Materials Technology

Dissertation was accepted for the defence of the degree of Doctor of Philosophy in Chemistry and Materials Technology on September 29, 2009

Supervisor: Leading Research Scientist Mare Altosaar, Department of Materials Science, Tallinn University of Technology

Opponents: Dr. Charlotte Platzer-Björkman, Uppsala University

Senior Researcher Dr. Ants Lõhmus, University of Tartu

Defence: November 9, 2009 at 14:00
Lecture hall: VI-121
Tallinn University of Technology, Ehitajate tee 5, Tallinn

Declaration:
Hereby I declare that this doctoral thesis, my original investigation and achievement, submitted for the doctoral degree at Tallinn University of Technology, has not been submitted for any academic degree.

/Kaia Ernits/

Ultraheli pihustuspürolüüsi ja keemilise sadestamise meetodil kasvatatud In$_2$S$_3$ ja ZnS õhukeste kilede uurimine

KAIA ERNITS

TABLE OF CONTENTS

LIST OF PUBLICATIONS

The present thesis is based on the following publications, which are referred to in the text by their Roman numerals.

I. K. Ernits, D. Brémaud, S. Buecheler, C.J. Hibberd, M. Kaelin, G. Khrypunov, U. Müller, E. Mellikov, A.N. Tiwari. Characterisation of ultrasonically sprayed In_xS_y buffer layers for Cu(In,Ga)Se$_2$ solar cells. Thin Solid Films 515 (2007) 6051.

II. K. Ernits, M. Kaelin, D. Bremaud, T. Meyer, U. Müller and A.N. Tiwari. Ultrasonically sprayed In_2S_3 films for Cu(In,Ga)Se$_2$ solar cells. Proceedings of 21st EPSEC (2006) p. 1853.

III. E. Mellikov, M. Altosaar, M. Krunks, J. Krustok, T. Varema, O. Volobujeva, M. Grossberg, L. Kaupmees, T. Dedova, K. Timmo, K. Ernits, J. Kois, I. Oja Acik, M. Danilson, S. Bereznev. Research in solar cell technologies at Tallinn University of Technology. Thin Solid Films 516 (2008) 7125.

IV. K. Ernits, K. Muska, M. Kauk, M. Danilson, J. Raudoja, T. Varema, O. Volobujeva, M. Altosaar. Chemical bath deposition of ZnS films using different Zn-salts. Physics Procedia xx (2009) xxx, *presented in the conference E-MRS 2009*.

V. K. Ernits, K. Muska, M. Danilson, J. Raudoja, T. Varema, O. Volobujeva, M. Altosaar. Anion effect of zinc source to chemically deposited ZnS(O,OH) films. Submitted for publishing in Advances in Material Science and Engineering, MS no. 372708.v1.

In Appendix A, copies of these papers have been included.

AUTHOR'S OWN CONTRIBUTION

The contribution by the author to the papers included in the thesis is as follows:

I. In_2S_3 film deposition by USP, CBD-CdS deposition, ZnO sputtering, Ni/Al evaporation; analysis of In_2S_3 film (Profilometer, Spectrophotometer) and In_2S_3/CIGS solar cells (I-V, EQE); analysis of results and major part of writing.

II. In_2S_3 film deposition by USP, CBD-CdS deposition, ZnO sputtering, Ni/Al evaporation; analysis of In_2S_3 film (Profilometer, Spectrophotometer) and In_2S_3/CIGS solar cells (I-V, EQE); analysis of results and major part of writing.

III. Deposition of ZnS films, analysis of results and minor part of writing.

IV. Deposition of ZnS and CdS films by CBD, measurement of CISSe and CZTSSe solar cells I-V characteristics, analysis of results and major part of writing.

V. Deposition of ZnS films by CBD; analysis of ZnS (Spectrophotometer), measurement of CISSe and CZTSSe solar cells I-V characteristics, analysis of results and major part of writing.

LIST OF ABBREVIATIONS AND SYMBOLS

ΔEc	Gap between two energy level of the conduction band bottom
Ac	CH_3COO (acetate)
ALD	Atomic layer deposition
AM1.5	Air mass 1.5
CBD	Chemical bath deposition
CGS	$CuGaS_2$
CGSe	$CuGaSe_2$
CIGSe	$Cu(In,Ga)Se_2$
CIGSSe	$Cu(In,Ga)(S,Se)_2$
CIS	$CuInS_2$
CISe	$CuInSe_2$
CISSe	$CuIn(S,Se)_2$
CVD	Chemical vapour deposition
CZTS	Cu_2ZnSnS_4
CZTSe	$Cu_2ZnSnSe_4$
CZTSSe	$Cu_2ZnSn(S,Se)_4$
Eg	Energy band gap
EQE	External quantum efficiency
ETHZ	Eidgenössische Technische Hochschule Zürich
η	Solar cell efficiency
FF	Fill factor
HR-SEM	High resolution scanning electron microscopy
ILGAR	Ion layer gas reaction
I-V	Current-voltage
j_{SC}	Short-circuit current density
L	Ligand
MGL	Monograin layer
MOCVD	Metal-organic chemical vapour deposition
MOVPE	Metal-organic vapour phase epitaxy
NREL	National Renewable Energy Laboratory
PCD	Photochemical deposition
pK	Instability constant
PV	Photovoltaic
PVD	Physical vapour deposition
RF	Radio frequency
RT	Room temperature
SEM	Scanning electron microscopy
SLG	Soda lime glass
SR	Spectral response
TCO	Transparent conductive oxide
T_H	Heater temperature

T_S	Substrate temperature
TU	Thiourea
SILAR	Successive ionic layer adsorption and reaction
USP	Ultrasonic spray pyrolysis
UV	Ultra-violet
V_{OC}	Open-circuit voltage
XPS	X-ray photoelectron spectroscopy
XRD	X-ray diffractometry

INTRODUCTION

Indium sulphide (In$_2$S$_3$) and zinc sulphide (ZnS) are important materials for optoelectronic and photovoltaic applications [1, 2]. They can be used as buffer layers to substitute cadmium sulphide (CdS) in CuInSe$_2$ (CISe) based solar cells to avoid toxic cadmium and develop more environmentally friendly technologies for photovoltaic solar cells. Substitution of CdS by other materials is a research line to obtain cells with non-toxic elements and higher efficiency. Indium sulphide and zinc sulphide prepared by chemical deposition methods are possible candidates because they offer enhanced properties as buffer layers due to their high energy gap values (Eg = 2.1-2.9 eV and Eg = 3.6 eV for the indium and zinc compound, respectively [3] and [4]), transparency, and good film properties (compact, adherent, surface adjustment to substrate crystals).

ZnS is also an important II–VI compound semiconductor for other applications, such as planar wave-guides, deep-blue light emitting devices or a base material for phosphors [5]. There are many methods to fabricate ZnS thin films, such as chemical bath deposition (CBD), chemical vapour deposition (CVD), photochemical deposition (PCD), successive ionic layer adsorption and reaction (SILAR), spray pyrolysis, and the metal-organic vapour phase epitaxy (MOVPE) [6 – 11]. Among them, CBD has been proven to be the most suitable method to produce ZnS thin films for photovoltaic applications because of its capability to be applied efficiently, cost-effective and large-scale. In addition, this method is normally used under the atmospheric pressure (usually air) and at near ambient temperatures, making it preferable to conventional vacuum-based vapour phase techniques that require much energy [12]. Chemical deposition of ZnS thin films has been carried out in aqueous alkaline baths by many researchers [13–16]. In most of these studies, an ammonia solution and one complementary cation-complexing agent have been used. That is why the formation of hydrolysed species in the solution and the formation of Zn–O bonds in the structure of ZnS layer are inevitable in these basic media [17]. The anions in the different zinc salts used as zinc sources in the CBD process play also a role in the formation of ZnS films as additional complexing agents, forming Zn[Ligand]$_n$ (Zn[L]$_n$)complexes besides $[Zn(NH_3)_4]^{2+}$ and $[Zn(OH)_4]^{2-}$ in the chemical bath solution. There are only few data in the literature on the influence of different anionic species in the ZnS deposition solution on thin film growth and on ZnS parameters. In this thesis the main attention is paid to the process of ZnS film growth and the impact of the Zn precursor anion on the properties of the CBD-ZnS film.

Tetragonal In$_2$S$_3$ (III–VI chalcogenide, *n-type* semiconductor) is also an attractive material for optoelectronics, radiation detectors, and electrical switching applications [18 - 25] and as a possible candidate for the buffer layer in CISe-type solar cells. Normally, CBD-In$_2$S$_3$ deposition is performed in acidic media [26-28]

11

and therefore it is not preferable for CISe-type absorber materials since here the useful etching effects of the absorber material in alkaline media is missing [29].

In this thesis the regularities of In_2S_3 film growth from solutions containing soluble In salt and thiourea in alcoholic solution formed by ultrasonic spray pyrolysis (USP) are presented.

Since the present studies are aimed at the use of the deposited ZnS and In_2S_3 films as buffer layers in $CuInSe_2$ and $Cu_2ZnSnSe_4$ (CZTSe) type photovoltaic (PV) solar cells, the influence of the buffer layer deposition process on solar cell characteristics is also analysed and the results are presented in the thesis.

ACKNOWLEDGEMENTS

1. LITERATURE REVIEW AND AIM OF THE WORK

1.1 Role of the buffer layer in photovoltaic solar cells

Solar cells converting absorbed solar light energy into electrical energy by the photovoltaic effect consist of several stacked semiconductor compound layers. In hetero-junction solar cells between a *p-type* absorber layer and a *n-type* transparent conductive collector layer (here a transparent conductive semiconductor oxide (TCO)), a thin (ordinarily 10 to 100 nm) buffer layer is deposited. It has been found that the buffer layer plays multiple roles in PV solar cells. The main role of the buffer layer is to produce an optimal transparent front junction to the absorber. Buffer layers affect also stress-induced degradation and transient phenomena in $CuInSe_2$-based solar cells. An optimum cell performance is usually found when the TCO layer in contact with the CdS as the buffer layer is highly resistive or almost insulating.

Researchers have found that the optimisation of the *p-n* junction forming layers in solar cells is extremely critical and interactive; i.e., in order to reach the highest cell performance, layers have to be constantly re-optimised to achieve the best performance. A unique combination of optimum materials for maximum device performance does not exist. Rather, the interactive nature of the optimisation process suggests that in many instances materials with less than ideal properties have to be used to achieve the best device performance. [30]

For $CuInSe_2$- and CdTe-based solar cells, multi-layer transparent conductors (TCO-s, e.g., ZnO or SnO_2) are generally used in combination with a CdS buffer layer.

1.2 Requirements for the buffer layers in CuInSe$_2$-type solar cells

There are general requirements for the buffer material in CISe-type solar cells [31]:

1) it should be an *n*-type semiconductor material,
2) it must be a stable compound,
3) it should be very thin (30 – 100 nm) to minimise the absorption of photons,
4) it's band gap should be wider and fit to the absorber material's band gap to avoid an unfavourable barrier formation for the electron flow in the solar cell,
5) the lattice constants of the material should fit to the absorber layer lattice constants to avoid stress in the crystal lattice and to ensure a working *p-n* junction between CIS and ZnO.

The matching of the lattice constants in Figure 1.1 shows that ternary sulphides like $CuInS_2$ (CIS), $CuGaS_2$ (CGS) and Cu_2ZnSnS_4 (CZTS) match better the cubic ZnS and ternary selenides, like $CuInSe_2$ (CISe), $CuGaSe_2$ (CGSe) and $Cu_2ZnSnSe_4$ (CZTSe), match rather the cubic ZnSe and cubic CdS. The values of the lattice constants of the hexagonal CdS, CdSe and ZnS films are in between the values of the p-type absorber and the *n-type* ZnO window layer, thus they should function as well as intermediate layers. The values of the lattice constants of the In_2S_3 are higher than the values for the absorber, therefore the role of In_2S_3 as a buffer layer is questionable at that point.
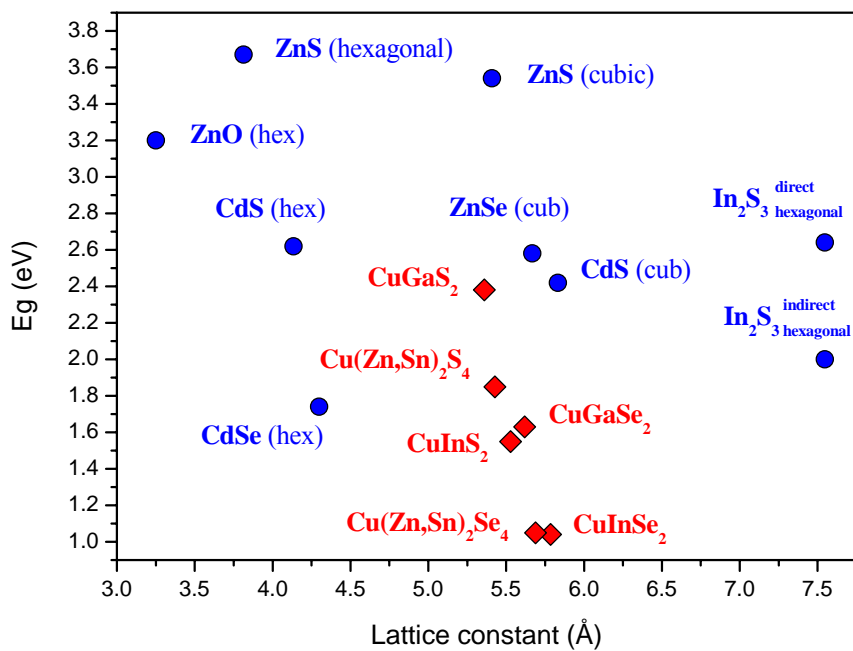
Figure 1.1. Band gaps and lattice constants of some semiconductor materials: absorber materials (red diamonds), buffer materials (blue circles)

A wider band gap of the buffer material is preferable to avoid absorption of photons, but if the energy level of the conduction band bottom is higher for the buffer material ($\Delta E_C > 0$), a "spike" will appear (Fig. 1.2) in the *p-n* junction. High spikes can impede photoelectrons and limit current in solar cells. However, if $\Delta E_C < 0$, a "cliff" appears (Fig. 1.2) and as a result, solar cell voltage is limited [32].
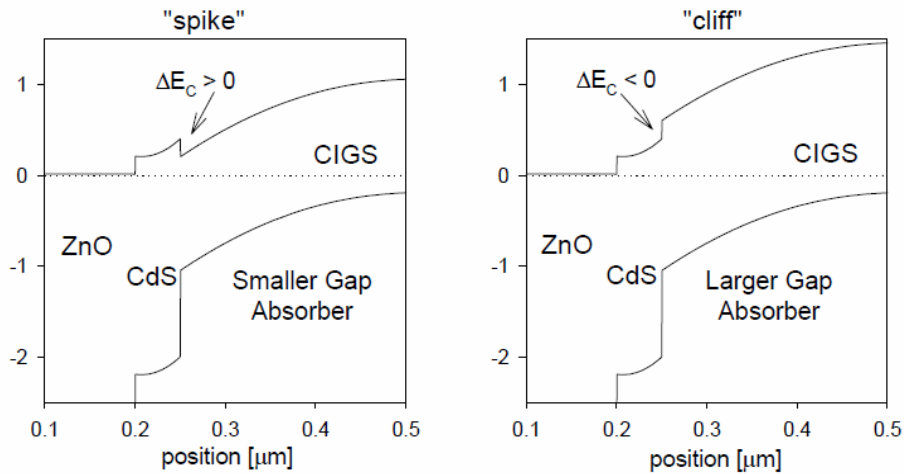
Figure 1.2. Conduction band offset problems in solar cells [32]
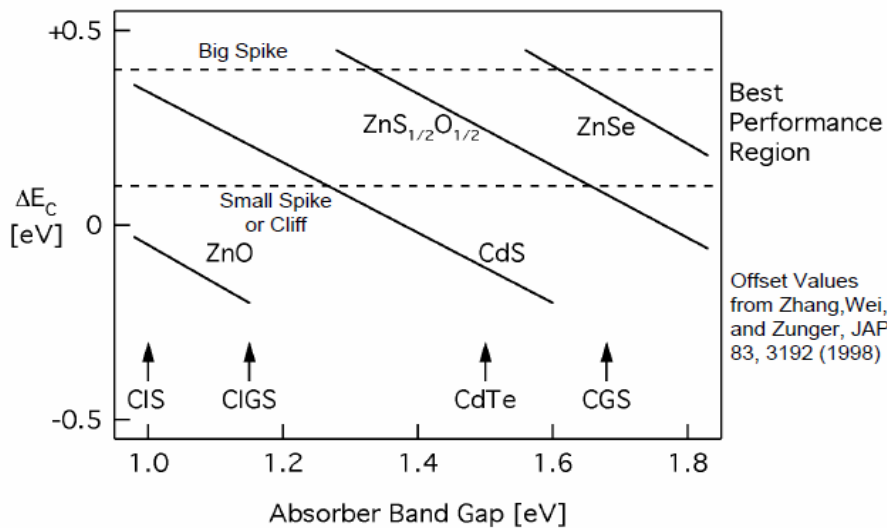
Figure 1.3. How to match absorber and buffer materials so that ΔE_C is in an optimal range [32]

Sites et al. [32] have found the best performance region of the ΔE_C for the solar cells (Fig. 1.3). According to the band gaps of the materials, CdS and In_2S_3 are most suitable for CISe, CIGSe and SZTSe absorber materials (Eg between 0.9 – 1.3), Zn(S,O) is preferable for CIS (Eg between 1.3 – 1.65), ZnSe for CGSe and CZTS (Eg between 1.65 – 1.9), but ZnS for CGS (Eg > 2.0).

1.3 Buffer layer materials for CISe-type solar cells

There are many buffer layer materials reported for CISe type material solar cells, like CdS, CdSe, ZnS, ZnO, ZnMgO, ZnSe, In_2S_3, In_2Se_3, $ZnInSe_x$, SnS_2, SnO_2, Bi_2S_3, Bi_2Se_3, Sb_2S_3, As_2S_3, HgS [33, 34]. Most investigated are CdS, ZnS, In_2S_3, ZnSe and ZnO. Some physical properties of CdS, ZnS and In_2S_3 materials are compared here.

1.3.1 Cadmium sulphide

The highest efficiency of CIGSe-type solar cells - 19.9 % is obtained with CBD-CdS [35]. CdS belongs to the group of II-VI semiconductor compounds. CdS is an *n-type* semiconductor with a band gap of 2.42 and 2.62 eV for cubic and hexagonal structures, respectively [36]. The lattice constants are a = 5.832 Å (cubic) and a = 4.135 Å, c = 6.75 Å (hexagonal) at room temperature (RT) [37]. The colour of CdS varies from transparent greenish yellow to orange yellow.

CdS exists in three crystal structures: wurtzite (hexagonal), zincblende (cubic) and rocksalt (cubic, exists only at very high pressure). The first two phases are difficult to distinguish and a mixture of both phases is often reported in chemically deposited thin films [38]. The CdS film can grow amorphous, polycrystalline or epitaxial, but the growth mode depends mainly on the substrate structure. The most common orientation of the films is (002) and (111) according to the crystal structure of the deposited film (hexagonal and cubic). (112) $CuInSe_2$ as an absorber material fits very well with both (111) cubic and (001) hexagonal CdS. The difference of the lattice parameters is 1.2 % between hexagonal CdS and CISe and 0.7 % between cubic CdS and CISe [39, 40]. Despite better fitting for meta-stable cubic CdS, the hexagonal modification of CdS is preferable since it is more stable [38, 41].

The average grain size of chemically deposited CdS on CISe is usually 10 to 20 nm, it can be several times larger if the pH value of the chemical bath solution is varied since a mixture of hexagonal $Cd(OH)_2$ and CdS is depositing at lower pH values: the size of the crystals of hexagonal $Cd(OH)_2$ is 100 to 1000 nm [38, 42].

Cd-compounds are considered harmful for human health; therefore a part of the solar cell society is looking for new alternative buffer layers. ZnS and In_2S_3 are good candidates for replacing CdS in CISe type solar cells [33, 43].

1.3.2 Zinc sulphide

So far, the highest efficiency achieved for a solar cell using ZnS is 18.6 % for CBD-ZnS/CIGSe, as reported by NREL [33]. ZnS belongs to the group of II-VI semiconductor compounds. The colour of ZnS varies from transparent to light yellow.

Zinc sulphide exists in zinkblende (cubic) and wurtzite (hexagonal) forms. ZnS is an *n-type* semiconductor with a band gap of 3.54 eV (cubic) and 3.67 eV (hexagonal) and its lattice constants are $a = 5.409$ Å (cubic) and $a = 3.814$ Å, $c = 6.26$ Å (hexagonal) at RT [37]. The cubic form is stable at RT, while wurtzite, the less dense hexagonal form, is stable above 1020 °C at atmospheric pressure, although there are hexagonal structures reported in chemically deposited thin films also at lower temperatures [44]. The cluster size of wurtzite ZnS in chemically deposited thin films is around 4 – 5 nm. CBD-ZnS deposits often with larger clusters during the chemical deposition and contains ZnO and $Zn(OH)_2$. It is reported that the ZnO cluster size is several times larger (up to 200 nm) [38].

1.3.3 Indium sulphide

The efficiency of an atomic layer deposited (ALD) In_2S_3/CIGSe solar cell reached as yet is 16.4 %, followed by chemical bath deposited (CBD) In_2S_3/CIGSe with 15.7 % [33]. In_2S_3 belongs to the group of III_2-VI_3 semiconductor compounds. In_2S_3 is a semiconductor with a band gap of 2.15 eV (indirect) and 2.64 eV (direct), lattice constants are $a = 7.62$ Å, $c = 32.33$ Å for β-tetragonal In_2S_3 [18, 45]. It was found that β- In_2S_3 with a direct band gap has *n-type* conductivity and is a suitable buffer layer material [46, 47]. The colour of In_2S_3 varies from transparent greenish yellow to orange yellow.

Several crystalline phases have been reported for In_2S_3 films (α-cubic, β-cubic, β-tetragonal and γ-tetragonal) as deposited by various techniques, with the β-tetragonal phase being the most stable at room temperature. This is the most common crystalline phase observed for In_2S_3 films [48]. The grain size of sprayed In_2S_3 thin films is found to be between 8 and 182 nm [45, 49], it increases with the substrate temperature.

One reason why CBD is not the most suitable for In_2S_3 deposition is that the CBD-In_2S_3 deposition takes place in acidic media [26 – 28] and the preferred ammonia-etching effect of the substrate of the absorber material is missing [29].

1.4 Absorber materials in CISe type solar cells

There are three different generations of solar cells: 1) first generation cells consist of large area, high quality and single junction devices, like crystalline silicon cells; 2) second (or thin film) generation materials have been developed to address energy requirements and production costs of solar cells, like CdTe, CISe and amorphous silicon solar cells; 3) third generation technologies aim to enhance poor electrical performance of the second generation while maintaining very low production costs, multi-junction (tandem) solar cells and concentrators [50]. CISe type solar cells belong to the group of the second generation, high-efficiency and low-cost thin film material solar cells. Most commonly investigated are $CuInSe_2$,

CuInS$_2$, CuGaSe$_2$ and Cu(In,Ga)Se$_2$ materials. Quaternary compounds have been reported recently, to substitute expensive indium and gallium with more common materials, like tin and zinc resulting Cu$_2$ZnSnS$_4$ (CTZS) and Cu$_2$ZnSnSe$_4$. All of them are stable semiconductor materials, with a direct band gap 1.0 - 1.65 eV, resulting theoretically in high efficiency of solar cells [51].

Although it is possible to make *p-n* homo-junctions of CISe, these are neither stable nor efficient. Therefore buffer layers are used to have a good contact between *p*-type CISe and *n*-type ZnO to form an efficient and stable hetero-junction solar cell. The typical structure of a thin film CISe type solar cell is given in Figure 1.4.
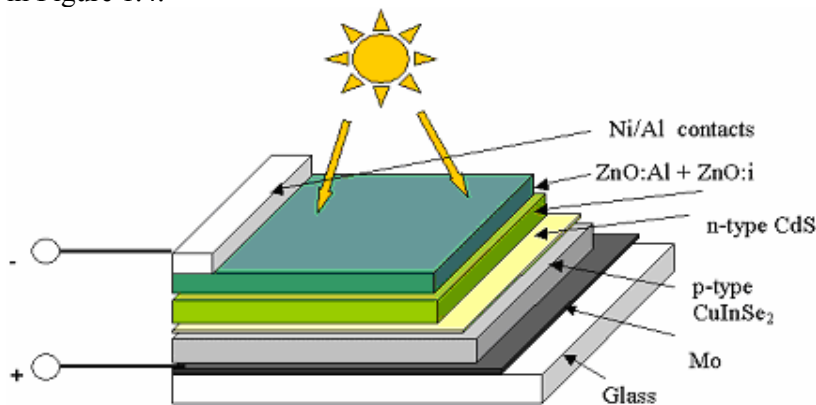
Figure 1.4. Typical structure of a thin film CISe solar cell [52]

The maximum efficiency for the 2nd generation thin film solar cell achieved is 19.9 % for a vacuum co-evaporated CIGSe with a chemically deposited CdS buffer material [35]. Thin film solar cells have achieved good efficiency only if high cost vacuum equipment is used. An alternative non-vacuum technology for producing CISe type materials, the technology of monograin powders, is investigated in the Laboratory of Semiconductor Materials Technology of Tallinn University of Technology. The efficiency of a CuInSe$_2$/CdS monograin layer solar cell reached by the research group is up to 9.5 % [53]. An efficiency of 5.9% for the Cu$_2$ZnSn(S,Se)$_4$/CdS monograin layer solar cell has been certified in the Fraunhofer Institute for Solar Energy Systems.

1.4.1 Properties of Some CISe-type materials

In this section mainly band gap values and lattice parameters of different CISe-type absorber materials are compared, the results being summarised in Figure 1.5 (a). The band gaps of absorber materials are influencing solar cells efficiencies, as shown in Figure 1.5 (b), because the materials are absorbing photons of the solar spectrum differently.
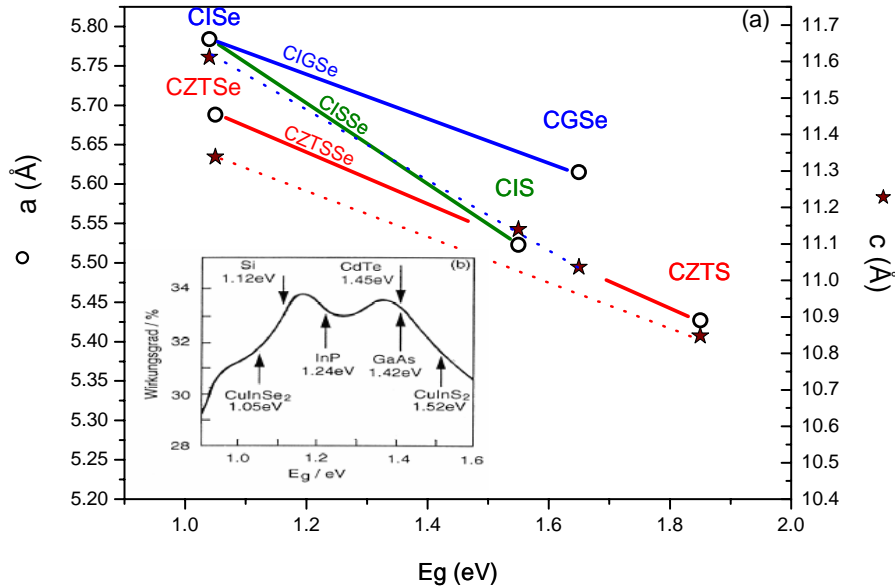
Figure 1.5. (a) Lattice parameter values as a function of band gaps of some CISe-type materials; (b) theoretical solar cell efficiency maximum as a function of the band gap energy under standard AM1.5 global irradiation [51]

CuInSe$_2$ and CuInS$_2$

CuInSe$_2$ and CuInS$_2$ belong to the family of I-III-VI$_2$ semiconductor materials that crystallise in the tetragonal chalcopyrite crystal structure. The values measured for lattice parameters of CISe at room temperature are a = 5.784 Å and c = 11.612 Å and for the CIS are a = 5.523 Å and c = 11.140 Å [54, 55]. CISe is a direct band gap material with a band gap of 1.04 eV [56] and CIS has a band gap of about 1.55 eV [57], which are both close to the optimum for the solar spectrum, as shown in Figure 1.5 (b) [51]. Materials with an even better band gap can be found between CIS and CISe, therefore varying the concentrations of sulphur and selenium of the material can improve CuIn(S,Se)$_2$ (CISSe) the (theoretical) solar cell efficiency.

CISe and related compounds are interesting materials for the solar cell community due to the extremely high absorption coefficient ($\alpha(h\nu) = 2\cdot10^5$ cm^{-1}), which allows complete sunlight absorption in just a few micrometer thin layer of the material [51].

Cu(In,Ga)Se$_2$

The lattice parameters of CIGSe are primarily influenced by the [Ga]/[In] concentration ratio, it varies from $a = 5.784$ Å, $c = 11.624$ Å (for CuInSe$_2$) to $a = 5.615$ Å and $c = 11.036$ Å (for CuGaSe$_2$) [58]. The band gap of CIGSe is around 1.2 eV, but can vary from 1.04 eV (CISe) to 1.65 (CGSe).

Cu$_2$ZnSnS$_4$ and Cu$_2$ZnSnSe$_4$

Cu$_2$ZnSnS$_4$ and Cu$_2$ZnSnSe$_4$ are less investigated I$_2$-II-IV-VI$_4$ semiconductor materials. The measured values of the lattice parameters of CZTS are: $a = 5.427$ Å and $c = 10.848$ Å [59]. CZTS has a direct band gap of $1.40 - 1.82$ eV [60 – 63], close to the optimum value for PV applications. The material also has a high optical absorption coefficient ($\alpha(h\nu) \sim 10^4$ cm^{-1}). CZTSe lattice parameters are $a = 5.688$ Å and $c = 11.338$ Å [64] and it has energy band gap values from $1.05 - 1.44$ eV [63, 65, 66]. The optimum band gap material can be obtained when varying the relative concentrations of sulphur and selenium in the Cu$_2$ZnSn(S,Se)$_4$ (CZTSSe) solid solution material.

1.5 Methods for growing thin film buffer layers

Thin films have been grown by various techniques, such as physical vapour deposition (PVD) [67], atomic layer deposition (ALD) [2], metal-organic chemical vapour deposition (MOCVD) [68], evaporation, sputtering, chemical bath deposition (CBD), ion layer gas reaction (ILGAR), and spray pyrolysis [33]. CBD, ILGAR [69, 70] and spray pyrolysis (SP) techniques are preferable for industrial applications because of the economical, non-vacuum systems involved.

In this thesis the chemical bath deposition for growing CdS and ZnS thin films and the ultrasonic spray pyrolysis for growing In$_2$S$_3$ thin films are used.

1.5.1 Ultrasonic spray pyrolysis

The advantage of the spray pyrolysis method is that it is a fast, material-efficient, large-area scalable and simple method for growing thin film layers in which the deposition parameters can easily be varied [18, 45, 71 – 74].

In an ultrasonic spray pyrolysis (USP) system, an alcoholic solution containing the precursor salts is nebulised by an ultrasonic actuator and then transported to a heated substrate, where the reaction between precursors takes place to form a thin film.

The alcohols are used as solvents because of their lower boiling temperature than water, therefore the solvent evaporates faster from the substrate and the film can grow faster and denser.

The advantage of the USP over conventional pneumatic spraying is the better control of the spray flux with a soft carrier gas flow, which allows the deposition of very thin layers with even thickness. The solution droplet size is smaller in USP, but the mist can be easily affected by the air or exhaust turbulence. The control of the thickness is important for thin buffer layers in CISe type solar cells where the desired film thickness is 30 – 100 nm.
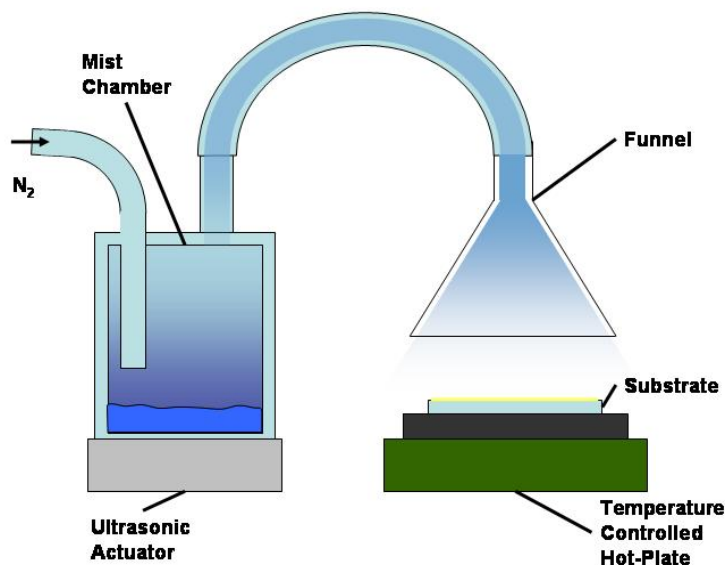
Figure 1.6. Schematic of the USP system

The USP system setup is shown in Figure 1.6, where the mist of the solution generated by the ultrasonic actuator is transported through a tube and the funnel for spray deposition.

The substrate temperatures used in USP (> 200 ˚C) are higher than those in the CBD process (< 100 ˚C), therefore not all solar cell constructions can use the USP (e.g. monograin layers containing organic compound materials).

In$_2$S$_3$ films by USP

According to the literature, In$_2$S$_3$ films have been deposited from spray solutions containing InCl$_3$ and CS(NH$_2$)$_2$ (TU – thiourea) salts, the solvent being usually a mixture of water and different alcohols [18, 45, 71 – 74]. Nitrogen was used as the carrier gas in most cases and substrate temperatures were kept in the range of 150 – 380 °C.

The reaction for the USP-In$_2$S$_3$ formation is considered as an oxidation reaction (1.1):

$$2InCl_3 + 3CS(NH_2)_2 + 4CH_3OH + 2O_2 \rightarrow In_2S_3 + 6NH_4Cl + 3CO_2 + 2H_2O \quad (1.1)$$
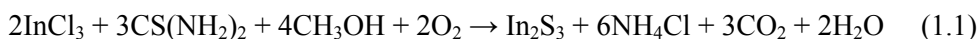
It was found by Abou-Ras et al. that high substrate temperatures influence the interface between CIGSe and In_2S_3 and lead to the formation of an interfacial layer with defective structure and unfavourable electronic characteristics due to the inter-diffusion of copper and indium [67]. These effects together resulted in a decrease of the solar cell efficiency for cells with the buffer layer grown at high temperature (380°C).

The $[InCl_3]/[TU]$ ratio in the spray solution and the substrate temperature impact on the composition and on optical and electrical properties of the In_2S_3 films were studied in most cases. It was found that the preferential orientation is along the (220) plane when the substrate temperature or the sulphur concentration in the solution is increased. The value of the direct band gap of the film decreases with increasing the sulphur concentration [45]. The lattice constants and the indirect band gap of the sprayed In_2S_3 increased with the sulphur concentration in the films [18]. The indirect optical band gap was found to be in the range of 2.15 – 2.43 eV and the direct band gap in the range of 2.64 – 2.81 eV.

The impurities in the semiconductor films decrease the carrier mobility and therefore are not favourable. Oxygen is an isovalent substitute for sulphur or can change the stoichiometry of the material. Chlorine is a donor type dopant in In_2S_3 and can increase the conductivity of the material.

1.5.2 Chemical deposition

Chemical deposition refers to the deposition of sparingly water-soluble elements and compounds on a solid substrate from a reaction occurring in an aqueous solution. Chemical deposition of films is not a new technique. As early as 1835, Liebig reported the first deposition of silver using a chemical solution technique [38].

The chemical bath deposition (CBD) is one of the most common and cheapest methods for growing thin continuous semiconductor films like CdS and ZnS. It is popular because of its simple process and instruments.

The simplest experimental set-up for CBD film preparation is shown in Figure 1.7. A vessel with heated water is used to heat up the bath solution, constantly stirred during the deposition process. The substrate can be added and removed at any time during the process.

At first sight the seemingly simple process involves several possible reactions and mechanisms for growing a semiconductor film. There are several parameters to control (like choosing the precursors, concentration, pH and temperature of the solution) and to find proper conditions of the deposition.

A solution for chemical deposition contains a metal salt, a chalcogen source and a complexing agent. $M(CH_3COO)_2$, MCl_2, MI_2, $M(NO_3)_2$ or MSO_4 salts are used as sources of metal ions (M = Cd, Zn). NH_4OH and its salts are often used as complexing agents. Thiourea ($CS(NH_2)_2$, also written as TU) or thioacetamide are used as a sulphur source in alkaline and acidic solutions, accordingly.
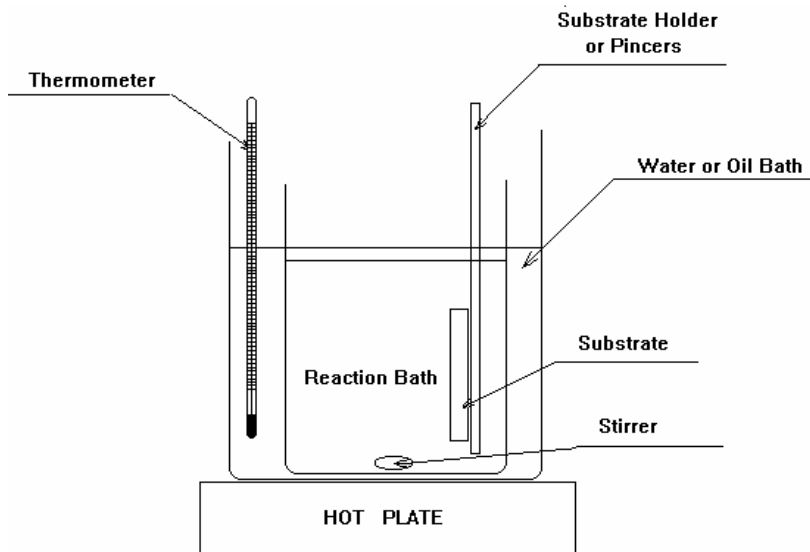
Figure 1.7. Experimental setup for chemical bath deposition [75]

Although the reactions involved in the CBD process appear to be quite straightforward, the exact mechanism of the CBD process is often unclear. The reason is that there can be several different mechanisms, like ion-by-ion, cluster-by-cluster and mixed precipitation [76, 77]. Below is shown a simple ion-by ion mechanism, using the common thiourea deposition of CdS as an example [38]:

$$Cd(NH_3)_4{}^{2+} \leftrightarrow Cd^{2+} + 4\ NH_3 \qquad\qquad (1.2)$$
$$SC(NH_2)_2 + 2OH^- \leftrightarrow S^{2-} + 2H_2O + H_2CN_2 \qquad\qquad (1.3)$$
$$Cd^{2+} + S^{2-} \rightarrow CdS \qquad\qquad (1.4)$$
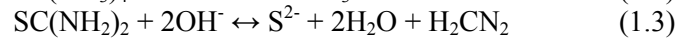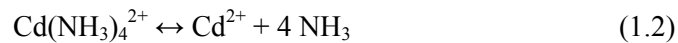
In a first step, the dissociation of $Cd(NH_3)_4{}^{2+}$ complex liberates Cd ions (1.2), then the formation of a sulphide ion occurs (1.3) and finally the CdS forms by ionic reaction (1.4).

Doping in CdS and ZnS films

Doping can be divided into two parts: native doping by changing stoichiometry and extrinsic doping by foreign elements. Doping leads to modified carrier concentration, dark resistivity and photoconductivity of the CdS and ZnS films [38].
Boron, chlorine and iodine are well known as donor type impurities in CdS and ZnS. The dark resistivity drops by nearly three orders of magnitude with an optimum B content (B:Cd concentration ratio in the solution of 0.001) [78]. Aluminium, as a trivalent ion, should act as an *n*-type dopant for CdS. A small

decrease in resistivity was found when $Al_2(SO_4)_3$ was added to a chemical bath [79].

ZnS by CBD

ZnS is commonly deposited by CBD [44, 77, 80 – 85]. However, in many cases, the deposited ZnS film is not stoichiometric and contains oxygen (probably as zinc hydroxide or oxide) and the deposited product is often written as ZnS(O,OH) [15, 86 – 88]. Activation energies for ZnS depositions are generally considerably lower than for CdS deposition and this suggests a mechanism different from that of the CdS deposition. The crystal size of ZnS is usually smaller than that of CdS. Both of these factors suggest that ZnS forms by a pure cluster mechanism [38].

Here is the simple cluster (hydroxide) mechanism, using the common thiourea-deposition of ZnS as an example [38]:

$$n(Zn^{2+} + 2OH^-) \leftrightarrow [Zn(OH)_2]_n \qquad (1.5)$$
$$[Zn(OH)_2]_n + nS^{2-} \rightarrow nZnS + 2nOH^- \qquad (1.6)$$
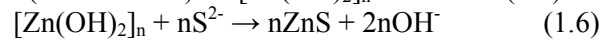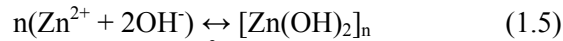
First, the formation of a solid $[Zn(OH)_2]_n$ cluster occurs (1.5), then S^{2-} ions from the reaction (1.3) form and join into a nS^{2-} clusters. ZnS formation takes place as described by the exchange reaction (1.6).

Ennaoui et al. [80] found that the insertion order of the precursor chemicals into the CBD solution plays a major role in controlling the chemical route of the ZnS formation. Usually a Zn salt and ammonia are inserted into the solution at the same time and the $[Zn(NH_3)_4]^{2+}$ complex forms in the solution. The $[Zn(NH_3)_4]^{2+}$ complex decomposes after the addition of thiourea. Otherwise, when Zn salt and TU are inserted together, the $[Zn(SC(NH_2)_2)_4]^{2+}$ complex forms first, resulting in sulphur rich ZnS films without any oxygen in the films.

The most known ZnS(O,OH) deposition recipe was published by Nakada [89], in which (0.1 – 0.3 M) $ZnSO_4$, (0.4 – 0.8 M) TU and (10.5 – 11.0 M) NH_3 is used to deposit 100 nm ZnS layer on top of CIGSe. Since the CIGSe solar cell with ZnS(O,OH) had higher quantum efficiency in the short wavelength region and therefore resulted in higher current densities, a higher solar cell conversion efficiency of 16.9 % (17.2 % after light soaking) was achieved with the ZnS(O,OH) layer, while the efficiency of a similar CIGSe with the CdS layer was 16.8 %. The record conversion efficiency of 18.6 % for a CIGS/ZnS(O,OH) device with a multi-layer CBD-ZnS(O,OH) deposited by the Nakada process was reported by Contreras [90].

It was found by Zhou et al. [91] that the resistance and transmission of the ZnS films decreased and the film thickness increased with increasing the concentration of $ZnSO_4$ in the CBD solution. Another group found that by increasing $Zn(CH_3COO)_2$ and TU concentrations at the same time so that the ratio of Zn:S was fixed, a thicker ZnS films was compared to those grown from solutions with lower concentrations. The thickest films grew when the ammonia concentration in

the solution was 8 Mol/L [92]. An increase of pH and a decrease of the temperature of the chemical solution slow down the film growth process during the deposition. Investigation of the effect of temperature on the size of nanocrystallites and the value of band gap energy showed that the crystallite sizes increase and the band gap energy value decrease with the increase of the solution temperature between 25 and 75 ºC. Ennaoui et al. [93] found that a ZnS buffer layer prepared at 50 ºC lead to the highest Cu(In,Ga)(S,Se)$_2$ (CIGSSe) solar cell fill factor, open circuit voltage and efficiency in the studied temperature range of 40 – 70 ºC.

Heat treatment was used in many cases to improve the crystallinity of ZnS(O,OH) films. Vidal et al. [94] used annealing in H$_2$ atmosphere at 200 ºC for 1 hour, and as a result, annealing decreased the band gap energy of CBD-ZnS film by 0.18 eV and increased slightly the conductivity of the films. Another study of H$_2$ annealing of ZnS films for 1 hour in the temperature range of 200 – 350 ºC showed a decrease of the film transmission by increasing annealing temperatures [95].

Several studies on CBD ZnS in different chemical bath concentrations, pH and temperature have been reported, but the impact of the Zn-salt anion effect in alkaline solution has as yet been adequately studied.

Anion effects in chemical deposition

Some influences of different anions of Cd-salts on the CdS crystal growth were found previously. Several studies on the effect of anions on the growth rate and morphology of CdS films found small, but significant differences, which were more or less in agreement with [96, 97]. The latter found the growth rate to increase in the order: CdI$_2$, CdSO$_4$, Cd(NO$_3$)$_2$, Cd(CH$_3$COO)$_2$ and CdCl$_2$. This series corresponds approximately to the decreasing strength of the complexation of Cd^{2+} by the respective anions.

Khallaf et al. [98] supposed that the anion in the Cd salt plays a role in the growth of CdS film as a complementary complexing agent forming a Cd[anion]$_n$ complex besides [Cd(NH$_3$)$_4$]$^{2+}$ and [Cd(OH)$_4$]$^{2-}$ complexes in the chemical solution. They compared the instability constants of several complementary Cd complexes with the CdS growth rate and found that the growth rate of CdS films decreases with the increasing instability constants of complementary Cd[anion]$_n$ complexes.

Instability constants (reciprocal of stability constant) were calculated for several chlorine-cadmium complexes in the CdCl$_2$ solution. The complexation process was described as the following series of partial-reactions [99, 100, 101]:

$$1.7) \ CdCl^+ \leftrightarrow Cd^{2+} + Cl^- \quad K_1 = \frac{[Cd^{2+}][Cl^-]}{[CdCl^+]} = 2.86 \cdot 10^{-2},$$

$$pK_1 = -\log K_1 = 1.54$$

$$1.8) \ CdCl_2 \leftrightarrow CdCl^+ + Cl^- \quad K_2 = \frac{[CdCl^+][Cl^-]}{[CdCl_2]}, \ pK_2 = -\log K_2 = 2.06$$

1.9) $CdCl_3^- \leftrightarrow CdCl_2 + Cl^-$ $\quad K_3 = \dfrac{[CdCl_2][Cl^-]}{[CdCl_3^-]}$, $\quad pK_3 = -\log K_3 = 2.46$

1.10) $CdCl_4^{2-} \leftrightarrow CdCl_3^- + Cl^-$ $\quad K_4 = \dfrac{[CdCl_3^-][Cl^-]}{[CdCl_4^{2-}]}$, $\quad pK_4 = -\log K_4 = 2.00$
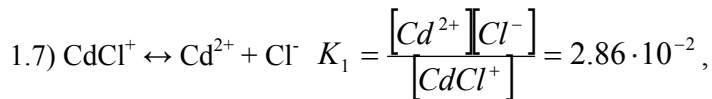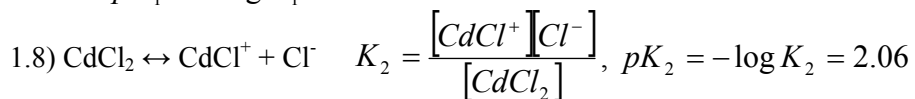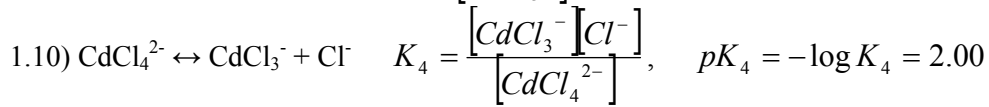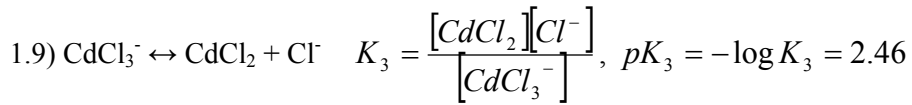
K_n (n = 1, 2, 3, 4) is the equilibrium constant of the n-th reaction. Square brackets imply the concentrations in (mol dm^{-3}). A high value of the instability constant pK_n shows that the ion is easily formed, therefore the complex ion with 3 chlorine atoms is the most stable complex in the series.

1.6 Summary of the literature review and objectives of the research

The highest CIGSe-type solar cell efficiency of 19.9 % is obtained if CdS deposited by a CBD process is used as a buffer layer [35]. CdS has been considered as the most suitable buffer material for CISe, CIGSe and CZTSe absorber materials also from a physical point of view [32].

Since CdS is considered harmful for human health, alternative buffer materials are gaining more focus. ZnS(O,OH) and $In_2(S,O)_3$ are two promising alternative buffer layer materials, but the deposition processes are not so thoroughly studied as for CdS. Both materials, ZnS and In_2S_3, have higher direct band gap energy values than CdS, that makes them more transparent in the short wavelength region and therefore more sunlight can be absorbed in the absorber material. Both materials, ZnS and In_2S_3, can be deposited onto the absorber material by chemical deposition methods: ZnS by chemical solution deposition (CBD) and In_2S_3 by ultrasonic spray pyrolysis (USP) methods.

It is known that anions of the different used Cd salts affect the formation of CdS films but the influence of different zinc sources on the CBD process of ZnS deposition is incompletely studied. Therefore one part of the present studies is dedicated to finding out the regularities of CBD-ZnS film growth and to the impact of Zn precursor anions on the CBD-ZnS film's properties. The other part of the studies is derived from an understanding that In_2S_3 deposition by the USP process from alcoholic solutions is promising, however, a process not yet studied in depth.

From an application point of view, the main objective is to find appropriate technologies for alternative buffer material deposition with the aim to substitute CdS in CISe and CZTSe type solar cells and to achieve comparable solar cell conversion efficiencies.

The study of the USP-In_2S_3 deposition was a new topic, since the USP setup was different from the conventional spray pyrolysis method used for the In_2S_3 deposition. Therefore the subject was:

- to investigate the optical, structural and compositional properties of USP-In_2S_3 films by varying the concentration of the solution and the temperature of the substrate;
- to prepare and study the properties of CIGSe solar cells with the USP-In_2S_3 thin film as a buffer layer, comparing them with those made with the standard CBD-CdS buffer layer.

The aims of the study of the CBD-ZnS deposition process were to find out the influence of different zinc precursors:
- on the growth of films and on the optical, morphological, compositional and electrical properties of the deposited films.
- to explore the impact of the anion effect on ZnS/CISSe and ZnS/CZTSSe monograin layer solar cells.

2. EXPERIMENTAL

CBD was used to grow ZnS(O,OH) films on top of $CuIn(S,Se)_2$ and $Cu_2ZnSn(S,Se)_4$ absorber material, because it is the most proven method for this purpose. We also found that the anion effect had yet not been studied for the ZnS(O,OH) deposition.

For the deposition of In_2S_3 films on $Cu(In,Ga)Se_2$ the USP technique was chosen, since $CBD-In_2S_3$ will waste too much precious indium and the $CBD-In_2S_3$ is deposited usually in acidic media, which is not preferable for CIGSe type material surfaces.

The experimental part of the thesis was conducted in two different institutions. The research of the $USP-In_2S_3$ deposition was performed in co-operation with the Thin-Film Physics Group in the Laboratory for Solid State Physics, ETH Zurich, Technopark, 8005 Zurich, Switzerland. The part of the deposition and the study of CBD-ZnS films was accomplished at the Chair of Semiconductor Materials Technology, Department of Material Science, Tallinn University of Technology, 19086 Tallinn, Estonia.

2.1 Ultrasonic Spray Pyrolysis

The USP set-up used for the In_2S_3 thin film deposition is described in more detail in section 1.5.1. Solaronix SA, Switzerland, provided the USP equipment.

2.1.1 Preparation of USP-In_2S_3 thin films

The In_2S_3 films were deposited on soda lime glass (SLG) substrates by spraying an alcoholic solution containing different concentrations of $InCl_3$ and $SC(NH_2)_2$ (TU). SLG substrates were cleaned with detergents, isopropanol and double deionised water. Various heater temperatures were used to produce layers for constant spraying time of 30 minutes (Table 3.1). The nitrogen carrier gas flow rate was kept at 1.5 l/min, corresponding to an average solution spray-rate of 40 ml/ 30 min.

2.1.2 Preparation of CIGSe/In_2S_3 solar cells

CIGSe absorber layers used for the production of thin film solar cells were grown by co-evaporation of elemental Cu, In, Ga and Se and using the "3-stage process" onto a Mo-coated SLG by colleague Dr. David Brémaud, as described elsewhere [102].

The In$_2$S$_3$ films were deposited on CIGSe substrates by spraying a methanol solution containing InCl$_3$ (0.005 M) and CS (NH$_2$)$_2$ (0.015 M). The CIGSe surface was activated by etching with 10 % KCN just before the buffer layer deposition. Various substrate temperatures (200, 220, 245 ºC) were used to produce layers for spraying times of generally 20 minutes. In order to have a buffer layer thickness smaller than 70 nm, on CIGSe substrates at a substrate temperature of 245 ºC a spraying time of 10 minutes was used. The nitrogen carrier gas flow rate was kept at 1.5 l/min, corresponding to an average solution spray-rate of 15 ml/ 10 min.

CBD-CdS was performed at a bath temperature of 70 ºC from an aqueous working solution containing 0.015 M Cd(CH$_3$COO)$_2$, 0.023 M TU and 1.336 M NH$_4$OH with a deposition time of 15 minutes for a standard buffer layer.

After USP-In$_2$S$_3$ or CBD-CdS buffer layer deposition onto the CIGSe, an i-ZnO/ZnO:Al window double layer was deposited by radio-frequency (RF) sputtering and a Ni/Al grid was physical vapour evaporated.

2.2 Chemical bath deposition

The CBD set-up used for the ZnS and CdS thin film deposition is described in more detail in section 1.5.2. IKA heating system thermocouple was used for keeping constant temperature in the water bath.

2.2.1 Preparation of CBD-ZnS thin films

The aqueous chemical bath contained ZnX$_n$ (0.016 M, X = CH$_3$COO, Cl, I, NO$_3$ and SO$_4$), NH$_4$OH (7.5 M) and CS(NH$_2$)$_2$ (0.32 M also marked as TU), the purities of some chemicals are presented in Table 2.1.

Table 2.1 Purities of some chemicals used for CBD-ZnS deposition

Compound	Provider	Purity
SC(NH$_2$)$_2$	Merck	99.0 %, pro analysi
Zn(CH3COO)$_2$·2H$_2$O	Merck	99.5 %, pro analysi
ZnCl$_2$	self prepared form metallic Zn and HCl (Fluka)	
ZnI$_2$	Merck	98.5 %, pro analysi
Zn(NO$_3$)$_2$·4H$_2$O	Merck	98.5 %, pro analysi
ZnSO$_4$·7H$_2$O	Merck	99.5 %, pro analysi

Certain concentrations for CBD-ZnS deposition were chosen after private discussion with my colleague Katri Muska. The ZnS films were deposited onto glass, Mo/glass and CIS substrates during 30 minutes (if not indicated otherwise) at various temperatures from 5 different zinc precursors. SLG substrates were cleaned with sulphuric acid and double deionised water. The other conditions of deposition,

like duration and precursor concentrations, have been studied previously and are not the subject of the current study.

2.2.2 Preparation of monograin layer CISSe/ZnS and CZTSSe/ZnS solar cells

CISSe and CZTSSe monograins were prepared as described elsewhere [53, 103, 104] by colleagues: Dr. Jaan Raudoja, Kristi Timmo and Katri Muska.

The CBD-ZnS films prepared from different zinc precursors and CBD-CdS as a reference were deposited on the CISSe and CZTSSe monograins during 5 and 15 minutes, respectively. The standard CdS chemical bath contained $Cd(Ac)_2$ (0.0014 M), TU (0.07 M), NH_4Ac (0.02 M), NH_4OH (0.02 M).

The monograin-layer (MGL) CISSe and CZTSSe solar cells were prepared by colleague Dr. Tiit Varema, as described elsewhere [105]. For the MGL formation, a monolayer of absorber powder crystals covered with a buffer layer was glued together by a thin layer of epoxy. After polymerisation of the epoxy, i-ZnO and conductive ZnO: Al were deposited by RF-sputtering onto the open surface of the layer. Solar cell structures were completed by vacuum evaporation of In grid contacts onto the ZnO window layer. Graphite paste was used for the back contacts.

2.3 Characterisation methods

USP-In_2S_3 and CBD-ZnS thin films and solar cells were characterised by the methods given in Table 2.2.

Table 2.2 Equipment used for the characterisation of the deposited thin films

Material/ Device	Material properties	Characterisation method	Details of the method	Operator
USP-In_2S_3 thin film	Thickness	Profilometer	DEKTAK 3030 Sloan	K. Ernits
	Optical transmission, band gap	Spectro-photometer	UV-160 Shimadzu	K. Ernits
	Elemental composition	XPS	Quantum 2000 PHI	Dr. U. Müller
	Phase composition	XRD		Dr. M. Kaelin
	Morphology	SEM	Supra 35	Dr. O. Volobujeva
CIGSe/In_2S_3 thin film solar cells	Solar cell output parameters	I-V	AM 1.5 (100 mW/cm^2)	K. Ernits

	SC light absorption	EQE	AM 1.5 (100 mW/cm²)	K. Ernits
CBD-ZnS thin film	Thickness, cluster size, morphology	HR-SEM	ULTRA 55 Zeiss	Dr. O. Volobujeva
	Elemental composition	XPS	Kratos Axis Ultra DLD Al Kα	M. Danilson
	Optical transmission, reflection band gap	Spectro-photometer	Jasco V-670 UV-VIS-NIR	K. Ernits
	Work function, resistivity	Kelvin probe	Kelvin Control 07 Besocke Delta Phi GmbH	K. Muska Dr. A. Mere
	Phase composition	XRD	Rigaku Ultima IV	Dr. A. Mere
CISSe/ZnS and CZTSSe/ZnS MGL SC	Solar cell output parameters	I-V	Keithley 2400	K. Ernits
	SC light absorption	SR		S. Moser M. Danilson

2.3.1 Calculation of the optical band gap

The optical absorption coefficient (α) was deduced from transmission and reflectance spectra using the relation

$$\alpha = -\ln(T_{cor}),\qquad (2.1)$$

where T_{cor} was calculated as

$$T_{cor} = T \cdot (1 - R) \qquad (2.2)$$

from the intensities of the transmitted (T) and reflected (R) light.

$$\alpha \cdot h \cdot v = A(h \cdot v - E_g)^{\frac{1}{2}}, \quad (2.3)$$

where hv is the photon energy, A is a parameter depending on the transition probability and Eg is the direct optical band gap of the material. A plot of the value of $(\alpha hv)^2$ – calculated from equation (2.3) – against photon energy (hv) shows a straight line portion, and the intercept of this linear portion on the energy axis at $(\alpha hv)^2$ equal to zero gives the band gap of the material.

2.3.2 Calculation of the Fermi level

Combining the results of the Kelvin probe and optical measurements, Fermi levels were calculated for the ZnS(O,OH) layers from the relation:

$$E_F = E_g + \chi - \Phi, \qquad (2.4)$$

where E_F is Fermi level, E_g - band gap energy, χ - electron affinity and Φ – work function, considering that $\chi = 3.9$ eV [106]).
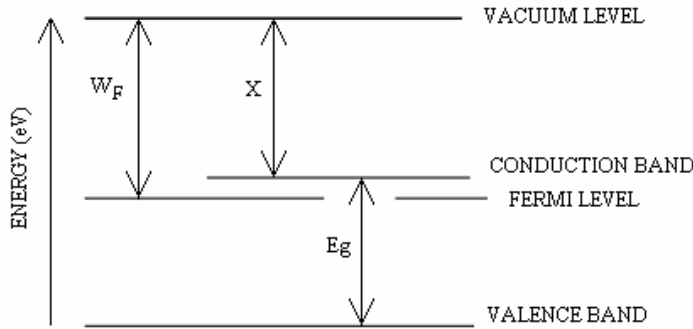
Figure 2.1. Energy diagram of an n-type semiconductor material. W_F denotes the work function, X – the electron affinity, E_g – the optical band gap of the material

2.3.3 Current density-voltage characteristics of solar cells

The most important parameter of a solar cell is its efficiency η. It is defined as the ratio of the maximum (electrical) power density delivered by the cell to the power density incoming from the light source. The additional characteristic cell parameters that are commonly used to describe the performance of the cell are the open circuit voltage (V_{OC}), the short-circuit current density (j_{SC}), and the fill factor (*FF*). Standard efficiency measurements use an air mass factor 1.5 (AM1.5) spectrum, which corresponds to standard terrestrial conditions (ASTM 1999) with an integrated irradiance power density of 1000 W/m^2, RT. These parameters are indicated in Figure 2.2 and explained in the following section.
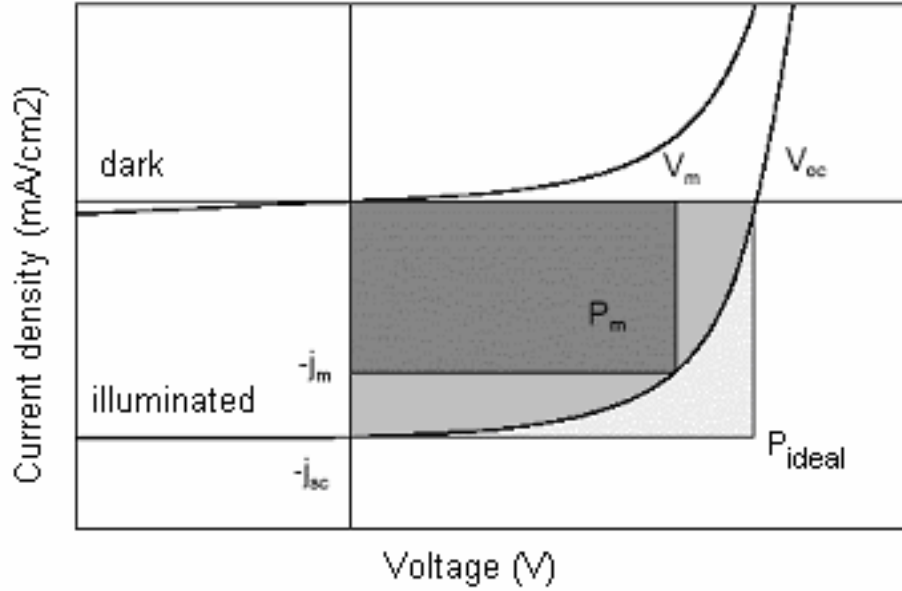
Figure 2.2. Solar cell current density-voltage characteristic under dark and illuminated conditions. The solar cell parameters j_{SC}, V_{OC} and the maximum power point $P_m(V_m, j_m)$ can be determined

The efficiency of the solar cell is the most informative parameter, since it contains all the other parameters calculated from Eq. (2.5):

$$\eta = \frac{j_{SC} \cdot V_{OC} \cdot FF}{P_{in}}, \qquad (2.5)$$

where P_{in} is the power of the standard illumination of AM 1.5 (100 mW/cm^2). *FF* is often used to characterise the quality of a solar cell junction, calculated by Eq. (2.6),

$$FF = \frac{j_m \cdot V_m}{j_{SC} \cdot V_{OC}}, \qquad (2.6)$$

where j_m is the current density at maximum power output and V_m is the voltage at maximum power output.

3. RESULTS AND DISCUSSION

3.1 Deposition of USP-In$_2$S$_3$ thin films

All the studied films were deposited on SLG substrates. Film preparation conditions are described in 2.1.1.

3.1.1 Study of USP-In$_2$S$_3$ thin films deposited at different substrate temperatures and with different [TU]:[InCl$_3$] ratios in spray solution

Growth of USP-In$_2$S$_3$

The temperatures and precursor concentrations in the spray solution used for the In$_2$S$_3$ film deposition and the measured film parameters are presented in Table 3.1.

The influence of the [TU]:[InCl$_3$] concentration ratio on the growth rate (layer thickness grown for a constant time period) of the deposited layers was studied at a constant substrate temperature of 220 ºC (Table 3.1). Table 3.1 shows that the growth rate is the highest if the concentration ratio [TU]:[InCl$_3$] is around 3 to 4 and the rate is about 40 % lower for the films with the ratios 2 and 6 for the constant [InCl$_3$]=0.01. Therefore the concentration ratio [TU]:[InCl$_3$] = 4 was chosen as the optimal for the study of the impact of the substrate temperature on the USP-In$_2$S$_3$ film deposition.

Table 3.1. Deposition process parameters of In$_2$S$_3$ films, deposition time is 30 min

Temp. of heater T_H (ºC)	Substrate temp .T_S (ºC)	[InCl$_3$] (M/L)	[TU]:[InCl$_3$] (in solution)	Film thickness* d (nm)	Film transmission* $T_{700-1100}$ (%)	[S]:[In] (in film)	Structure of In$_2$S$_3$ phase		
							α-c	β-c	β-t
310	200	0.005	4	40	97				
310	200	0.01	4	70	94	0.79	+	+	
310	200	0.1	4	115	83				
345	220	0.005	4	45	95				
345	220	0.01	2	55	69	0.74	+	+	+
345	220	0.01	3	88	77	0.77	+	+	+
345	220	0.01	4	85	86	0.77	+	+	
345	220	0.01	6	65	92	0.72	+	+	
345	220	0.1	4	120	82				
380	245	0.005	4	50	94				
380	245	0.01	4	120	75	0.74		+	+
380	245	0.1	4	180	81				

*(The values of average transmission and thickness given in Table 3.1 have statistical distribution due to experimental limitations, the values are therefore indicating only the trends.)

As shown in Table 3.1 and Figure 3.1, the USP-In_2S_3 film growth rate is dependent on the substrate temperature (T_S) and the precursor concentrations in the spray solution. At higher T_S and $InCl_3$ concentration the film thickness (d) is higher if the [TU]:[$InCl_3$] ratio is kept constant in the solution for the constant deposition time (30 min). The effects are less pronounced for lower concentrations of $InCl_3$.
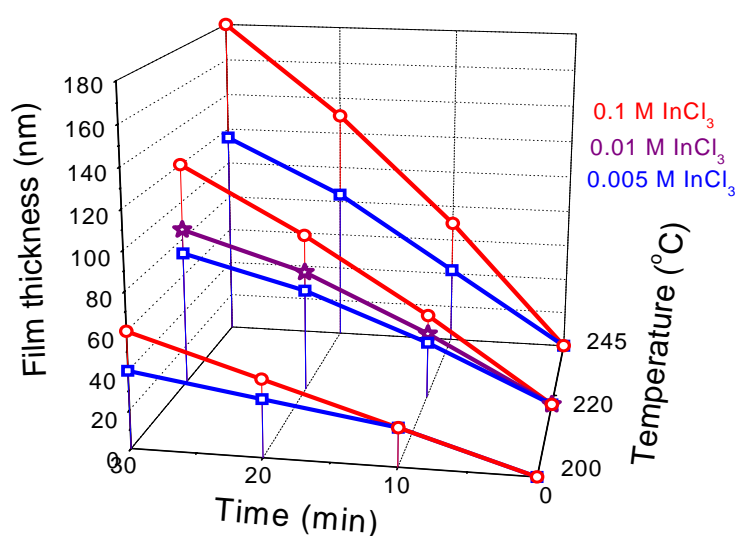
Figure 3.1. Dependence of USP-In_2S_3 film thickness on substrate temperature and $InCl_3$ concentration in the spray solution for constant deposition time 30 min

XRD and XPS study of USP-In_2S_3 films

As can be seen from the XPS depth profile (Fig. 3.2), the indium and sulphur concentrations are uniform throughout the layer. At the surface, carbon and oxygen are seen. Both impurities disappeared after 1 - 2 sputter cycles. We believe that they exist due to the adsorption and are simply surface contaminations. A chlorine impurity of around 1 at%, resulting from the use of $InCl_3$ salt, is present throughout the layer. The values of exact concentrations have not been calculated.
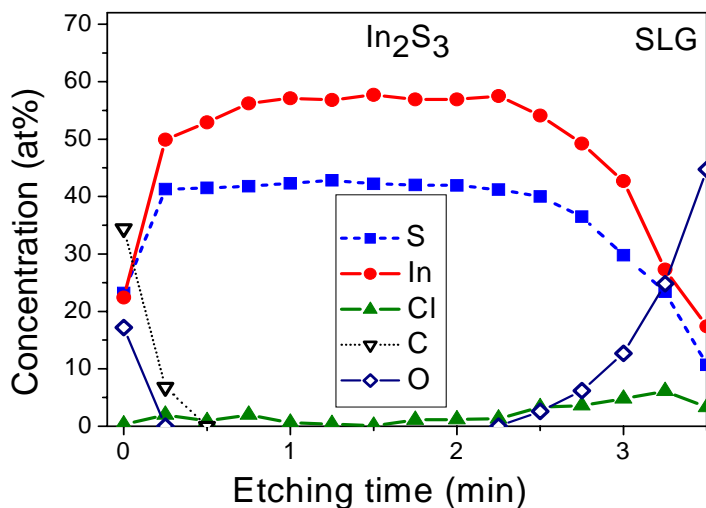
Figure 3.2. XPS depth-profile of USP-In₂S₃ film on SLG, sprayed at a substrate temperature of 220°C
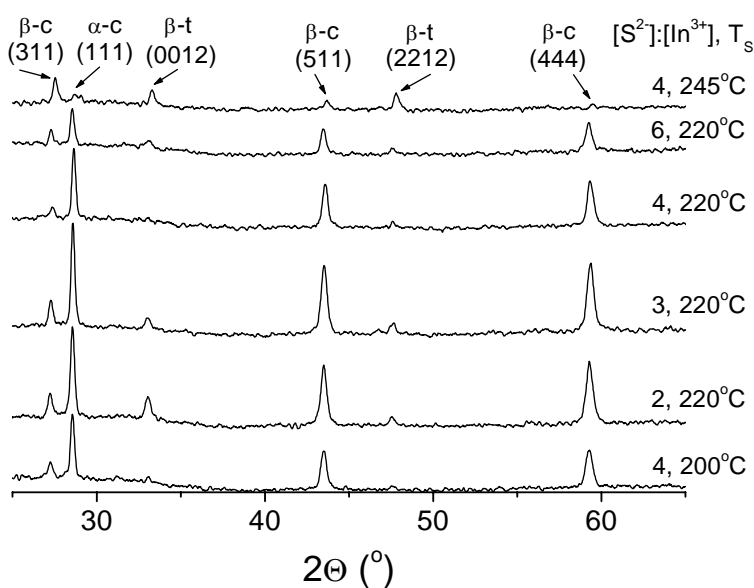
Figure 3.3. XRD patterns of USP-In₂S₃ films deposited at different substrate temperatures (TS) and different [TU]:[InCl₃] concentration ratios. The peaks of α-cubic (α-c), β-cubic (β-c) and β-tetragonal (β-t) In₂S₃ phases are marked following Ref. [107]

The dominating phases in the layers deposited at lower T_S are α-cubic and β-cubic In_2S_3 (Table 2.1, Figure 3.3). At higher T_S the peaks of the dominant β-tetragonal In_2S_3 phase are seen, accompanied with weak peaks of β-cubic In_2S_3. According to Gödecke et al. [108], the α-cubic phase forms in the studied temperature T_S region only if the sulphur concentration [S] is 59.7 – 60.0 at% in In_2S_3, while for the formation of the β–phase the [S] value is slightly lower ([S] = 58.6 – 59.4 at%). XPS measurements detected slightly lower S:In concentration ratio of 0.74 (Table 3.1) in the USP-In_2S_3 films for layers grown at higher T_S. The values of exact concentrations have not been calculated because standards were not available, therefore a relative change is given.

With an increasing [TU]:[$InCl_3$] concentration ratio the percentage of the β-tetragonal phase of ZnS(O;OH) films deposited in the substrate temperature of 220 ℃ decreases, as measured from XRD peak intensities (Figure 3.3).

Results of optical measurements

Figure 3.4 displays the optical transmission of films prepared at different TU concentrations in the wavelength region from 300 to 1100 nm. The [TU]:[$InCl_3$] concentration ratio influences the transmission of the deposited layers (Table 3.1). Film transmission decreases when the TU concentration in the solution was decreased. This can be due to the changes in the crystal structure of the layers, since the strongest tetragonal peak was found in the In_2S_3 films from a spray solution with the lowest TU concentration.
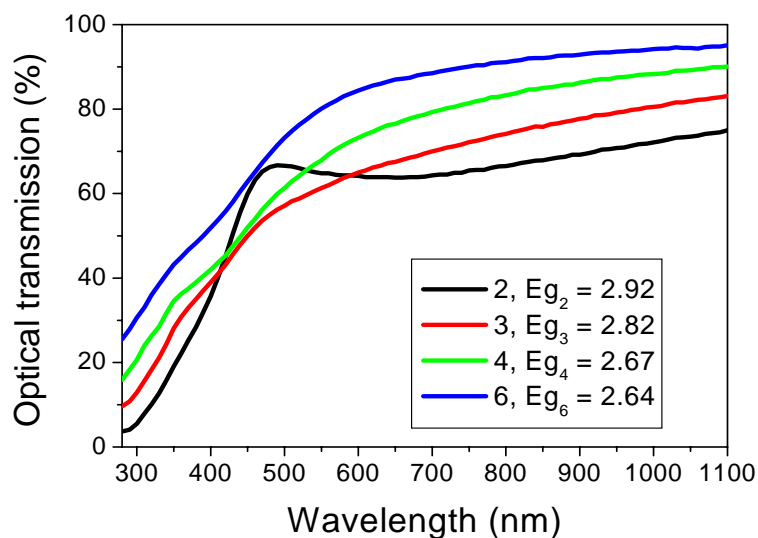
Figure 3.4. Optical transmission curves and optical band gap values of USP-In_2S_3 films deposited from spray solutions with different [TU]:[$InCl_3$] concentration ratios: 2, 3, 4 and 6. T_S=220 ℃; [$InCl_3$]=0.01 M

As the layers are very thin, only a rough estimate of the band gap energies can be given. However, it is clear that the absorption edge of In_2S_3 is in the region of 400 – 500 nm. Estimated In_2S_3 band gap values are between 2.6 – 2.9 eV and the values decrease with the increase of TU concentration in the spray solution (Fig. 3.4). This result agrees well with the experimental results of another study of SP In_2S_3 with a direct band gap [45].

The average optical transmission of the films decreases when T_S and $[InCl_3]$ increases, probably mainly due to the greater film thickness (see Table 3.1).

Morphology study with SEM

Figure 3.5 shows SEM images of an In_2S_3 layer sprayed on SLG from a solution containing 0.05 M $InCl_3$, $[TU]:[InCl_3] = 3$, $T_S = 220°C$ and a spraying duration of 60 minutes. It can be seen that the layer is continuous and that the thickness is approximately 170 nm (Fig. 3.5b). The surface of the film appears as polycrystalline with a grain size of 100 – 200 nm (Fig. 3.5a).
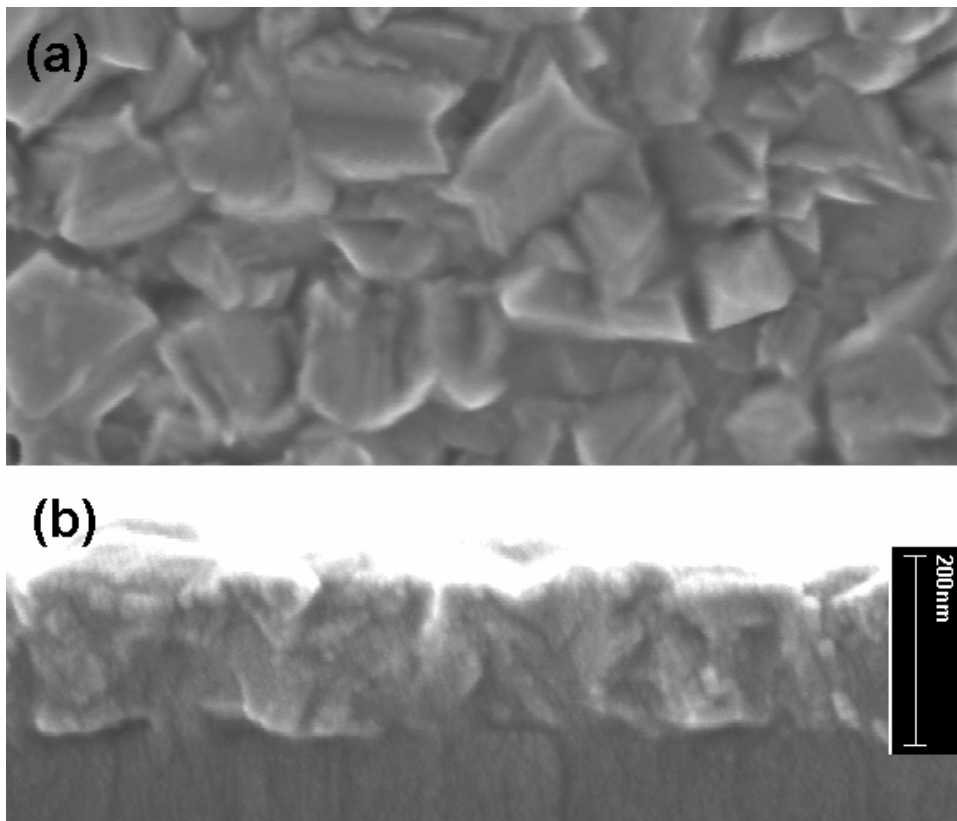
Figure 3.5. SEM images of an USP-In_2S_3 film on SLG: (a)surface and (b)cross-section. Grain size is 100 – 150 nm

Based on the results of the present study it can be concluded that the USP is a suitable method for growing thin In_2S_3 films in the range of substrate temperatures 200 – 245 ºC. The growth rate of the In_2S_3 films is higher at higher substrate temperatures and with higher precursor concentrations in the solution. The films contained indium and sulphur mainly, no oxygen was found inside the film. A small amount of chlorine is uniformly distributed in all samples. The sulphur concentration in the films decreases slightly with increasing substrate temperatures. The α phase is present in the films deposited at lower temperatures, while sulphur poor β-phase was dominating in In_2S_3 grown at 220 and 245 ºC. In the case of $[TU]:[InCl_3] = 2$ the shape of the optical transmission curve changed due to the different crystal structure. The values of the optical band gaps were lower in the higher values of the $[TU]:[InCl_3]$ ratio, and were in the range of 2.6 – 2.9 eV, which corresponds to the *n-type β-In_2S_3* with the direct band gap [47].

3.1.2 In_2S_3 as a buffer layer in comparison with CdS

The thickness and transmission of CBD-CdS films and of USP-In_2S_3 films sprayed at different temperatures for a fixed duration are given in Table 3.2. It can be seen that the film growth-rate increases with T_S. This is consistent with the optical transmission measurements (600 - 1100 nm): the films deposited at higher T_S are less transparent (the deposition duration was kept constant).

Table 3.2. Average thickness and average optical transmission (600 – 1100 nm) of In₂S₃
films sprayed for 20 minutes at different heater temperatures and data of a CdS film
deposited for 15 minutes in a chemical bath

Buffer layer	Substrate temperature (°C)	Film thickness (nm)	Optical transmission (%)
200°C In_2S_3	200	35	96.8
220°C In_2S_3	220	70	91.5
245°C In_2S_3	245	120	83.5
CBD-CdS	70	30	99.2

Figure 3.6 displays the optical transmission of USP-In_2S_3 and CBD-CdS films in the wavelength region from 300 to 1100 nm. As the layers are very thin, the band gap energies could be only roughly estimated. However, it is obvious that the absorption edge of CdS is in the region of 500 – 550 nm, while for In_2S_3 it is in the region of 400 – 500 nm, which corresponds to the *β*-In_2S_3 with a direct band gap. A rough estimation of the band gap values gave us 2.4 eV for CdS and 2.8 eV for In_2S_3 films.

Comparing the transmission spectra for the used buffer-layers with similar thickness (Fig. 3.6), it can be estimated that film transmissions are similar in the long wavelength region, but In_2S_3 has higher transmission in the blue light region.

As a result, it can be concluded that the optical properties of USP-In_2S_3 are suitable for the buffer layer in Cu(In,Ga)Se_2 solar cells.
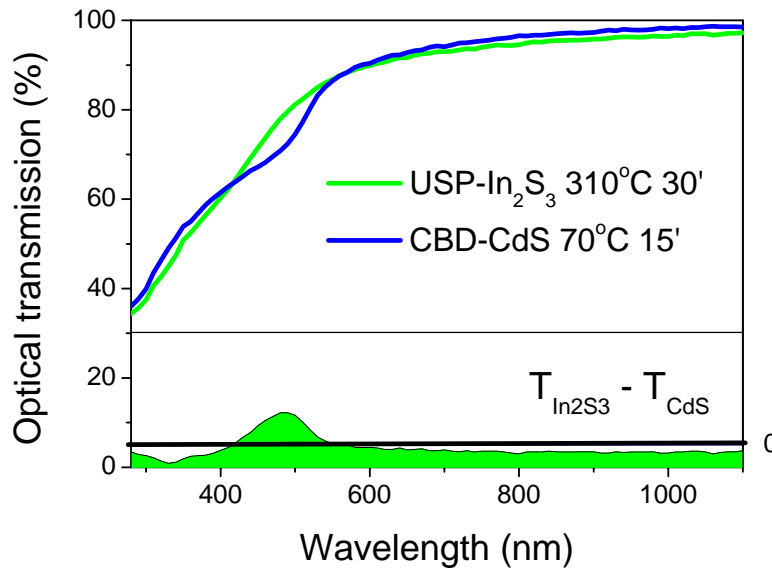
Figure 3.6. Optical transmission in the wavelength region 300 – 1100 nm
for a standard CBD-CdS film and for USP-In_2S_3 with a similar thickness

3.1.3 Cu(In,Ga)Se_2 solar cell characterisation

External quantum efficiency (EQE) measurements (Fig. 3.7 (a)) reveal the impact of CdS and In_2S_3 buffer layers on the solar cell light absorption and collection of photo generated carriers (Fig. 3.7 (b)). The most pronounced differences in the EQE occur in the wavelength region of 350 – 700 nm. The EQE of the In_2S_3/CIGSe cell is up to 15 % higher in the 350 – 500 nm (UV and blue light) region whereas the EQE of the CdS/CIGSe cell is up to 15 % higher in the 500 – 700 nm (visible light) region. This effect is due to the differences in the absorption characteristics of CBD-CdS and USP-In_2S_3. The USP-In_2S_3 band gap is apparently higher than the band gap of CdS, therefore more photons can pass through the buffer layer and reach the absorber layer.

Table 3.3 displays I-V characteristics for the best solar cells, namely the open circuit voltage (V_{OC}), the short-circuit current density (j_{SC}), the fill factor (*FF*), and the efficiency (η). The efficiency of the reference cell with CBD-CdS was 30 %

(relative) higher than the best efficiency obtained using the In_2S_3 buffer layer, mainly due to the higher values of V_{OC} and *FF*. Examining the impact of substrate temperature, V_{OC} increased slightly and *FF* decreased with the increasing substrate temperature, the latter being responsible for a drop in efficiency for the 245°C USP-In_2S_3/CIGSe solar cell.
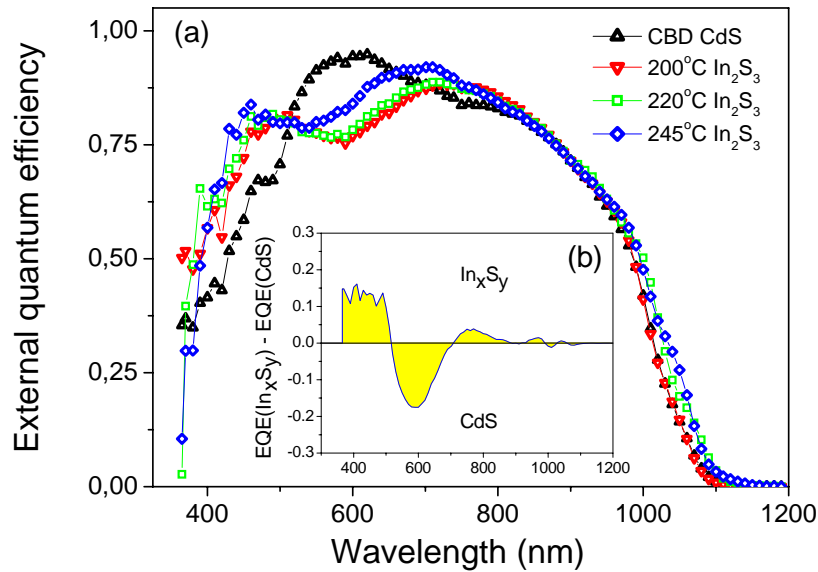
Figure 3.7. (a) Quantum efficiency measurements of CIGSe solar cells with different buffer-layers; (b) differences in spectral responses between solar cells with 220°C sprayed In_2S_3 and CBD-CdS buffer layers

Table 3.3. Current-voltage characteristics for CIGSe solar cells with different buffer layers

Buffer layer	V_{OC} (V)	j_{SC} (mA/cm^2)	FF (%)	η (%)
CBD-CdS	0.609	28.4	73.2	12.7
200°C In_2S_3	0.514	27.3	63.0	8.8
220°C In_2S_3	0.523	27.9	60.9	8.9
245°C In_2S_3	0.531	27.6	52.1	7.6

Although the USP-In_2S_3 has a wider band gap than CdS and thus absorbs less light in the short wavelength region, the current densities are comparable. The cells with the In_2S_3 buffer-layer have lower V_{OC} and *FF*.
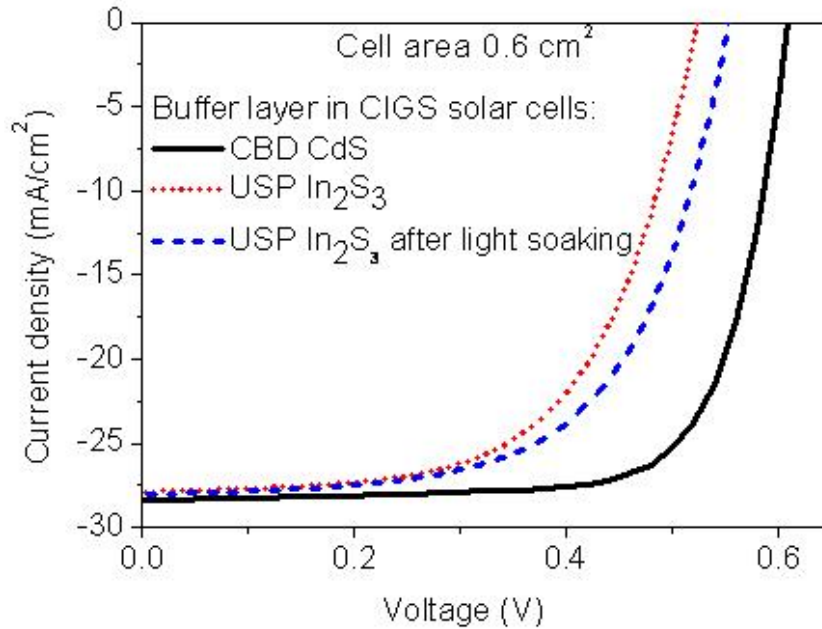
*Figure 3.8: I-V curves for solar cells with CBD-CdS and USP-In$_2$S$_3$
deposited at 220 ºC before and after 14 hours of light soaking*

Light soaking under AM1.5 illumination conditions was used to evaluate the stability of the In$_2$S$_3$/CIGSe solar cell and the results are presented in Figure 3.8. During 14 hours of light soaking the solar cell's *FF* and to a slightly lower extent its V_{OC} increased considerably, which resulted in the increase of the efficiency of the solar cell from 8.9 % (Table 3.3) to 9.5 % (V_{OC} = 0.552 V, *FF* = 61.8 %, J_{SC} = 28.1 mA/cm^2).

The high buffer-sensitivity to light soaking can be explained by enhancement in the In$_2$S$_3$/CIGSe interface quality [109]. The increase in V_{OC} may be caused by an increase in the effective carrier density [110]. The light soaking effect was reversible, which means that after keeping the cell in dark ambient, its efficiency decreased to the initial level. A similar effect has been reported for CIGSe solar cells with zinc-containing buffer layers, where the reversible improvement was made irreversible by using significantly higher irradiation intensities during the light soaking [109].

Open-circuit voltage dependence on temperature measurements (Fig. 3.9) shows that the compatibility between the In$_2$S$_3$ and the absorber is not as good as it is between the CdS and the absorber, because for In$_2$S$_3$ the value of *Voc* is lower at room temperature. In the case of compatibility the most important factor is the cleanliness of the *p-n* junction, which means that the interface between In$_2$S$_3$ and CIGSe is not working completely.
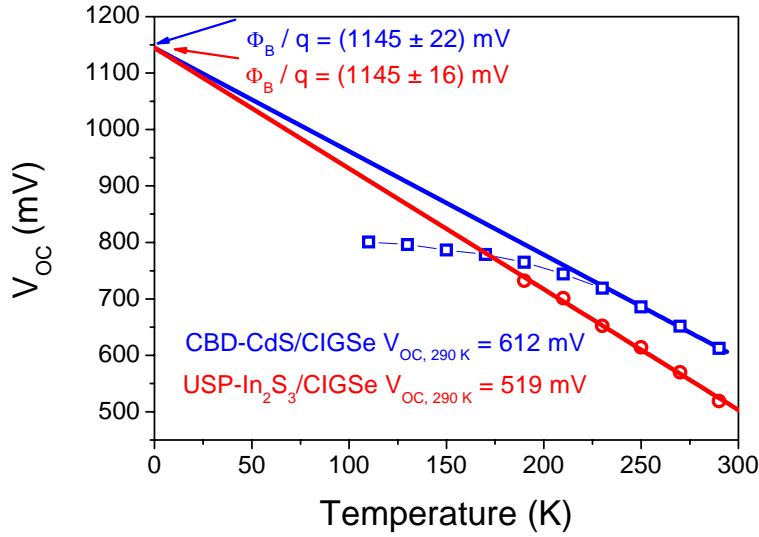
Figure 3.9. Open-circuit voltage dependence on temperature measurements for In_2S_3/CIGSe and CdS/CIGSe solar cells

The SEM cross-section (Fig. 3.10) shows the presence of about $30 - 50$ nm thin granular In_2S_3 layer between CIGS and ZnO layers. The conformal coverage of CIGSe surface appears rather poor for the USP-In_2S_3 buffer layer (Fig. 3.10 (a)), when CBD-CdS looks continuous and fits well with CIGSe and ZnO (Fig. 3.10 (b)).
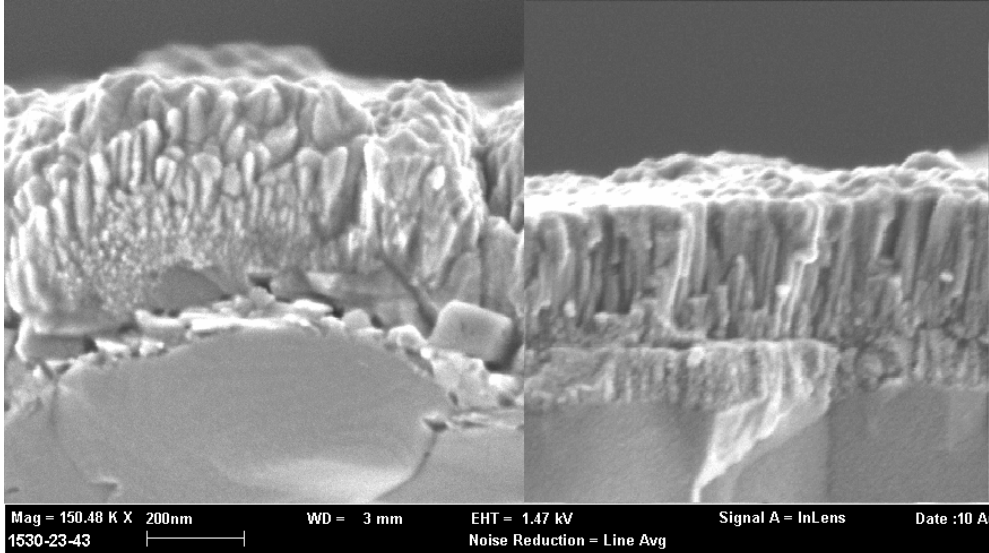
Figure 3.10: SEM cross-section image of the CIGSe solar cell with (a) USP-In_2S_3 and (b) CBD-CdS as a buffer-layer

Our initial trials to make CIGSe solar cells with very thin USP-In$_2$S$_3$ buffer-layers were successful, an efficiency of 9.5 % was achieved, but the cells were not as efficient as those with CBD-CdS buffer-layers (12.7 %). In the solar cells the USP-In$_2$S$_3$ layer appeared inhomogeneous with large grains on top of CIGSe. Further work should optimise the spray conditions for uniform coverage of CIGSe with thin USP-In$_2$S$_3$ layers. Additionally, further investigations of the interface properties are necessary to understand the reasons for low values of the open-circuit voltage and the fill factor in solar cells. Since the light soaking shows improvement of the solar cell, the post heat treatment should be investigated for the USP-In$_2$S$_3$/CIGSe solar cells. One option to improve the *p-n* junction is to use CIGSSe, which has higher band gap than CIGSe, and therefore fits better with In$_2$S$_3$.

This is the point where the author's work ends. Further investigations were done by Buecheler et al. [111]. The best cell efficiency of 12.4 % was obtained by them with the same USP-In$_2$S$_3$ spray deposition parameters: at 200 ºC for 15 minutes with 0.01 M InCl$_3$ and [TU]:[InCl$_3$] ratio of 4 in solution. The annealing treatment was performed at 200 ºC for 5 minutes on the finished solar cell devices with sulphur containing Cu(In,Ga)(S,Se)$_2$ absorber. The efficiency of the reference CBD-CdS/CIGSSe solar cell was 10.5 %. Therefore, the improvement in the efficiency of the solar cell was shown due to the improved *p-n* junction formation between sulphurised CIGSe absorber and USP-In$_2$S$_3$.

3.1.4 Summary of experimental results of USP-In$_2$S$_3$ study

USP is a suitable method for growing thin In$_2$S$_3$ films in the range of substrate temperatures 200 – 245 ºC. The growth rate of the In$_2$S$_3$ films is higher at higher substrate temperatures and with higher precursor concentrations in solution. The films contain indium and sulphur mainly, no oxygen was found inside the film. A small amount of chloride impurity is uniformly distributed in all samples. The sulphur concentration in the films decreased slightly with increasing substrate temperatures. The *α* phase is present in films deposited at lower temperatures, while sulphur poor *β*-phase was dominating in In$_2$S$_3$ grown at 245 ºC. In the case of [TU]:[InCl$_3$] = 2 the shape of the optical transmission curve changed due to the different crystal structure. The values of the optical band gaps were lower in the higher values of the [TU]:[InCl$_3$] ratio, and were in the range of 2.6 – 2.9 eV, which corresponds to the *n-type β*-In$_2$S$_3$ with a direct band gap.

Compared to CBD-CdS the optical properties of USP-In$_2$S$_3$ are more suitable for the buffer layer in Cu(In,Ga)Se$_2$ solar cells.

CIGSe solar cells with very thin USP-In$_2$S$_3$ buffer-layers achieved an efficiency of 9.5 % , but the cells were not as efficient as those with CBD-CdS buffer-layers (12.7 %). In solar cells the USP-In$_2$S$_3$ layer appeared inhomogeneous with large grains on the top of CIGSe. Further work should optimise the spray conditions for uniform coverage of CIGSe with thin USP-In$_2$S$_3$ layers. Additionally, further

investigations of the interface properties are necessary to understand the reasons of low values of open-circuit voltage and the fill factor in solar cells. Since the light soaking showed an improvement of the solar cells, the post heat treatment should be investigated for the USP-In$_2$S$_3$/CIGSe solar cells. One option to improve the *p-n* junction is to use CIGSSe absorber, which has higher band gap than the used CIGSe and therefore fits better with In$_2$S$_3$.

3.2 Deposition of CBD-ZnS(O,OH) thin films

In order to find out the optimal deposition conditions for ZnS(O,OH) chemical deposition we varied the temperature of the deposition solution, the precursor's inserting order and the nature of the precursor salt. The effect of different substrates on the morphology of CBD-ZnS films was also studied.

3.2.1 The study of the growth of CBD-ZnS(O,OH) films

The temperature impact on the growth rate of the deposition of CBD-ZnS(O,OH) onto CuInS$_2$/Mo substrates was studied using Zn(CH$_3$COO)$_2$ as a zinc precursor. Optimal deposition temperature was found around 80 ºC from Figure 3.11. Deposition rate was increasing with the temperature and slowed down at temperatures higher than 75 degrees due to prevalence of homogeneous precipitation of colloidal particles in solution. Therefore, thinner films were found to grow at lower degrees than 70 and higher than 80.
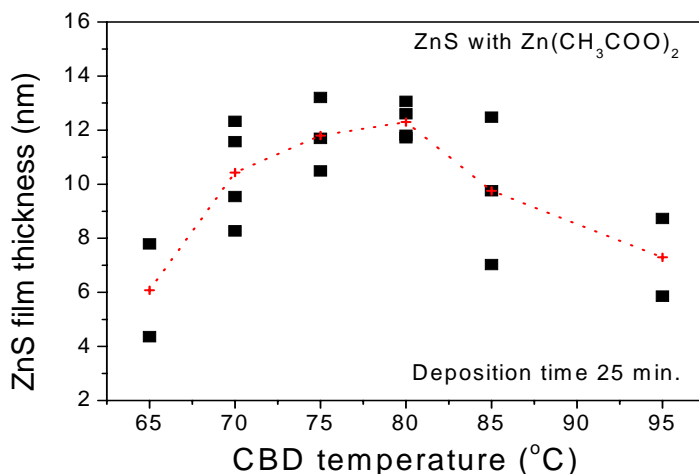
Figure3.11. CBD-ZnS(O,OH) film thickness at different deposition
temperatures, deposited during 25 minutes onto CuInS$_2$/Mo substrates

The inserting order of the precursor into the chemical bath solution in the temperature influence study was: 1) $Zn(CH_3COO)_2$, 2) NH_4OH and 5 minutes later 3) TU was added. In the literature it is reported that another inserting order, where TU was added before ammonia solution, increases ZnS concentration in CBD-ZnS films [80]. Therefore, the precursor's inserting order, where Zn-source and TU were added first, was used for the following experiments to have ZnS rich ZnS(O,OH) films.

In order to maintain the optimal (80 ºC) deposition temperature in the solution, a slightly higher temperature of the water bath (85 ºC) was chosen for the following research.

3.2.2 Study of ZnS(O,OH) films deposited from different zinc sources

Chemical route to ZnS(O,OH) deposition and the anion effect

In the chemical bath solution, Zn ions form different complex ions:

1) $2\,Zn^{2+} + 4\,CS(NH_2)_2 + 4\,NH_4^+ \leftrightarrow [Zn(CS(NH_2)_2)_4]^{2+} + [Zn(NH_3)_4]^{2+}$
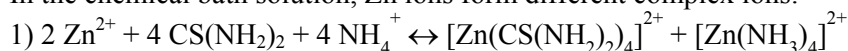
We assume that ZnS(O,OH) forms through the decomposition of the formed complexes by Eqs. (2) and (3):

2) $[Zn(CS(NH_2)_2)_4]^{2+} + 2\,OH^- \rightarrow ZnS\downarrow + CN_2H_2 + 3\,CS(NH_2)_2 + 2\,H_2O$

3) $[Zn(NH_3)_4]^{2+} + CS(NH_2)_2 + 2\,OH^- \rightarrow ZnS\downarrow + 4\,NH_3 + 2\,H_2O + CN_2H_2$
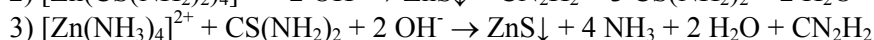
Simultaneously to ZnS formation, zinc hydroxide can form in the alkaline solution as follows :

4) $Zn^{2+} + 2\,OH^- \rightarrow Zn(OH)_2\downarrow$
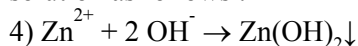
The deposited films were annealed in vacuum at 220 ºC for 10 minutes to dehydrate $Zn(OH)_2$ (5).

5) $Zn(OH)_2 \rightarrow ZnO + H_2O$ (T = 125 ºC [112])
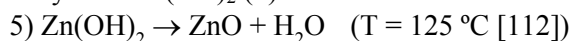
Table 3.4. Instability constants of Zn complexes [99]

Zn[L]n	pK (Instability constant)
$Zn[OH]^+$	4.40
$Zn[NH_3]^{2+}$	2.18
$Zn[SO_4]$	2.34
$Zn[CH_3COO]^+$	1.57
$Zn[Cl]^+$	-0.50
$Zn[I]^+$	-2.90
$Zn(NO_3)_2$	unstable, soluble compound

The anions of the used zinc salts play a role in the growth of ZnS(O,OH) films as additional complexing agents, forming $Zn[Ligand]_n$ ($Zn[L]_n$)complexes besides $[Zn(NH_3)_4]^{2+}$ and $[Zn(OH)_4]^{2-}$ in the solution. $Zn[L]_n$ complexes have different instability constants according to the anions, as shown in Table 3.4. When

comparing the pK values, it appears that the $Zn[SO_4]$ complex is stronger than $Zn[NH_3]^{2+}$ and other $Zn[L]_n$ complexes. This fact probably affects ZnS films growth in the way that the stronger $Zn[SO_4]$ complex turns Eq. (1) left, that could result in lower ZnS deposition rate. On the other hand, the $[Zn(OH)_4]^{2-}$ complex is still stronger and Eq. (4) goes right, resulting in $Zn(OH)_2$ richer films in the use of $ZnSO_4$ as a precursor. The instability constants were calculated for sparingly soluble compounds only, therefore the pK for $Zn[NO_3]^+$ complex is not given.

Effect of the substrates used

The deposition of ZnS(O,OH) films onto SLG, Mo/SLG and CIS/Mo results in different cluster sizes (Fig. 3.12, Table 3.5). ZnS(O,OH) deposits most poorly on SLG, with largest clusters (up to 330 nm). The coverage of ZnS(O,OH) on Mo substrates is slightly better and clusters are smaller (up to 270 nm), but $CuInS_2$ is covered by ZnS(O,OH) continuously with small clusters (in the range of 10 nm).

Table 3.5. Thickness and grain size of ZnS(O,OH) films deposited at 85 ºC for 30 minutes onto Mo and SLG substrates

Zn source	pH	Thickness on Mo (nm)	Cluster size on Mo (nm)	Cluster size on SLG (nm)
$ZnSO_4$	12.2	33	50 – 200	40 – 250
$Zn(Ac)_2$	12.1	82	70 – 270	100 – 330
$ZnCl_2$	11.9	67	40 – 150	35 – 140
ZnI_2	11.9	52	50 – 200	50 – 250
$Zn(NO_3)_2$	12.1	32	40 – 120	40 – 140

Thickness and cluster size of ZnS(O,OH) films deposited from different zinc precursors

SEM micrographs (Fig. 3.12.1-3.12.5) revealed that the usage of different zinc salts affects the ZnS(O,OH) cluster size and the film thickness of the films grown on SLG and on Molybdenum. The thickest films with the largest clusters were grown from solutions containing $Zn(Ac)_2$. ZnS(O,OH) films with the smallest clusters were grown from solutions containing $ZnCl_2$, but the thinnest films were deposited from solutions containing either $ZnSO_4$ or $Zn(NO_3)_2$, as can be seen in Table 3.5.

Figure 3.13 shows that film thickness is increasing with the pK values in the region (a) ($pK_{Zn(NH3)2+} > pK_{Zn(L)n}$) and drops after the $Zn[NH_3]^{2+}$ complex line, which is indicating to the decrease of ZnS(O,OH) growth rate in the region (b) ($pK_{Zn(L)n} > pK_{Zn(NH3)2+}$) where the value of Zn sources pK is higher than the value of $Zn[NH_3]^{2+}$ pK.
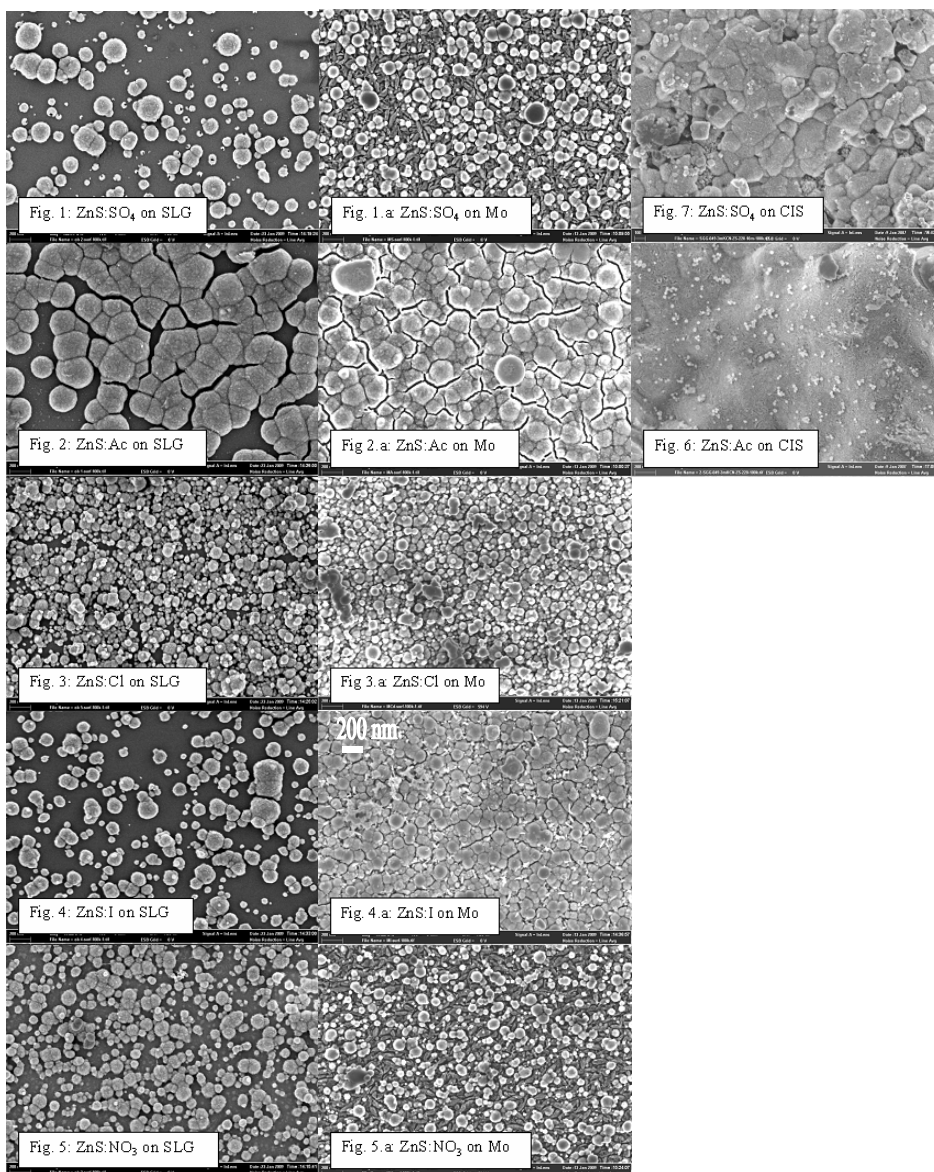
Fig. 3.12.1 – 3.12.7. SEM photos (100 000 x magnification) of ZnS(O,OH) deposits obtained from different zinc sources: 1) $ZnSO_4$, 2) $Zn(Ac)_2$, 3) $ZnCl_2$, 4) ZnI_2 and 5) $Zn(NO_3)_2$ deposited on SLG and Mo/SLG; and ZnS(O,OH) films from 6) $Zn(Ac)_2$ and 7) $ZnSO_4$ deposited onto CIS/Mo
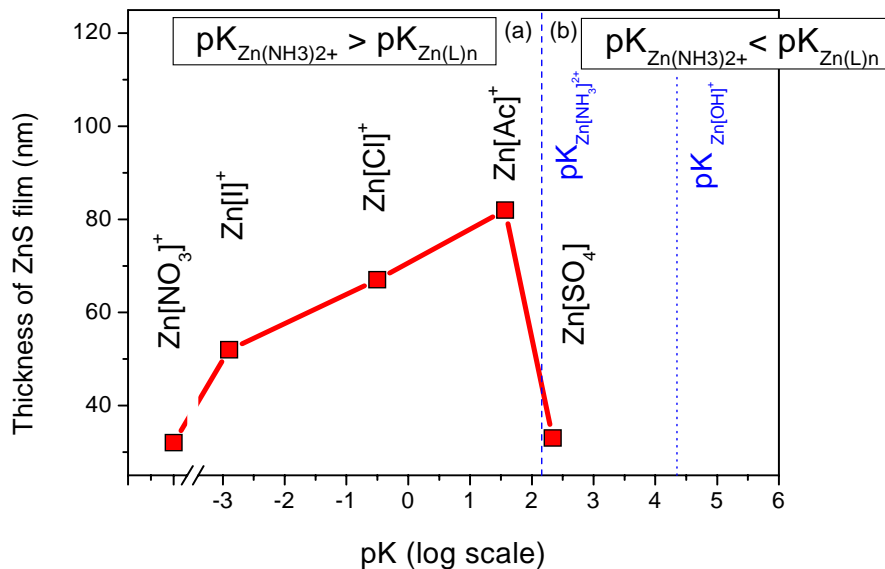
Figure 3.13. Thickness of ZnS(O,OH) films deposited from 5 different Zn-sources versus pK. The blue dashed line indicates $Zn[NH_3]^{2+}$ complex line, which divides the graph into two regions: (a) $pK_{Zn(NH3)2+} > pK_{Zn(L)n}$ and (b) $pK_{Zn(NH3)2+} < pK_{Zn(L)n}$. The blue dot line indicates $Zn[OH]^+$ complex line
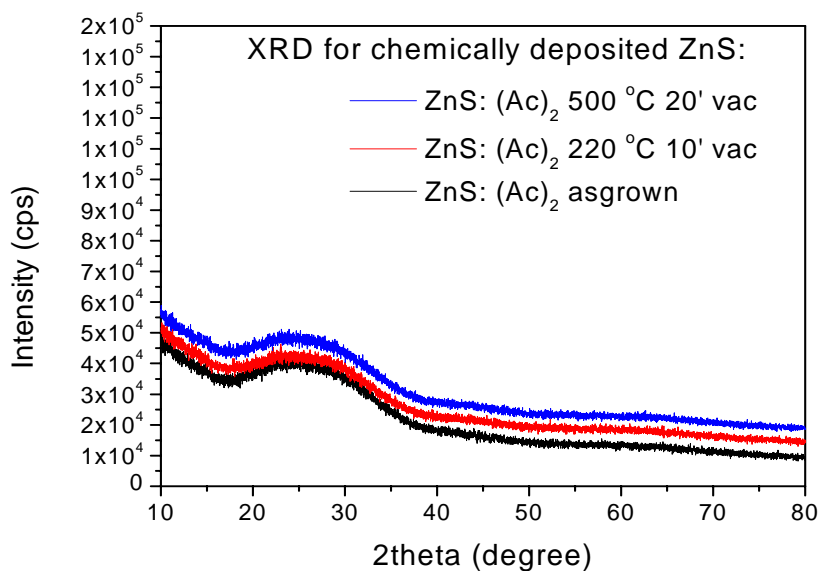
Figure 3.14. XRD difractogram for as-grown (bottom line) and 220 ºC (middle line), 500 ºC annealed ZnS(O,OH) films from Zn(Ac)₂

Compositional study of CBD-ZnS(O,OH) films from different precursors

Results of XRD measurements for ZnS(O,OH) films from zinc acetate show that as-grown and annealed films are amorphous (Fig. 3.14). We can find from the literature [98] that ZnS(O,OH) films deposited from $Zn(Ac)_2$ are often amorphous.

Table 3.6. Composition of ZnS(O,OH) deposits obtained from different zinc sources and determined by XPS-measurements

Composition Elements		XPS Peak (eV)	Used Zn anion source				
			$ZnSO_4$	$Zn(Ac)_2$	$ZnCl_2$	ZnI_2	$Zn(NO_3)_2$
Zn	(at%)	1022.0	37	40	46	43	43
S	(at%)	161.9	19	27	26	22	23
O (Me-O)	(at%)	530.4	13	6	9	8	9
O (-OH)	(at%)	531.6	31	27	19	27	25
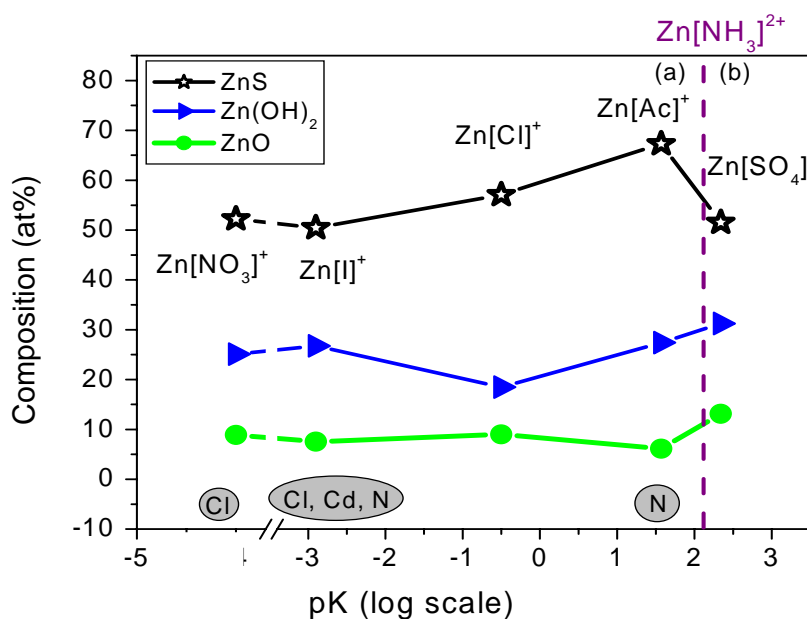
Figure 3.15. The composition of ZnS(O,OH) films versus pK of Zn complexes. The films contain mainly ZnS (stars), ZnO (circles) and Zn(OH)$_2$ (triangles). The dashed line indicates Zn[NH$_3$]$^{2+}$ complex line, which divides the graph into two regions: (a) pK$_{Zn(NH3)2+}$ > pK$_{Zn(L)n}$ and (b) pK$_{Zn(NH3)2+}$ < pK$_{Zn(L)n}$

XPS compositional measurements revealed that the ZnS(O,OH) films contain $Zn(OH)_2$ and ZnO besides ZnS. (Table 3.6). The concentration of ZnS in the ZnS(O,OH) films is given in Figure 3.15 (black stars). The obtained results show that the content of the ZnS in ZnS(O,OH) film is dependent on the instability

constant of the zinc precursor complex. The content of ZnS in the films increases with the value of pK of the $Zn[L]_n$ complex in the region (a) and drops after the $Zn[NH_3]^{2+}$ complex line in region (b). This is an indication of low deposition rate of ZnS and high deposition rate of $Zn(O,OH)_2$ in the region (b) where the $Zn[L]_n$ complex is stronger than the $Zn[NH_3]^{2+}$ complex.

XPS measurements revealed little but detectable amounts (below 1 at%) of impurities (grey rings in Fig. 3.15) in ZnS(O,OH) films from $Zn(NO_3)_2$ (Cl), ZnI_2 (Cd, Cl, N) and $Zn(Ac)_2$ (N).

XPS measurements showed also that the annealing in vacuum at 200 ºC for 10 minutes was not sufficient to dehydrate $Zn(OH)_2$ completely. As a result of the compositional study of the CBD-ZnS films, the deposited films are marked as ZnS(O,OH).

Optical transmission and band gap measurements of the ZnS(O,OH) films

The results of optical transmission measurements are provided in Figure 3.16 (squares). In region (a) film transmission decreases with increasing pK values and increases after the $Zn[NH_3]^{2+}$ complex line in region (b) where $pK_{Zn(L)n} > pK_{Zn(NH3)2+}$.
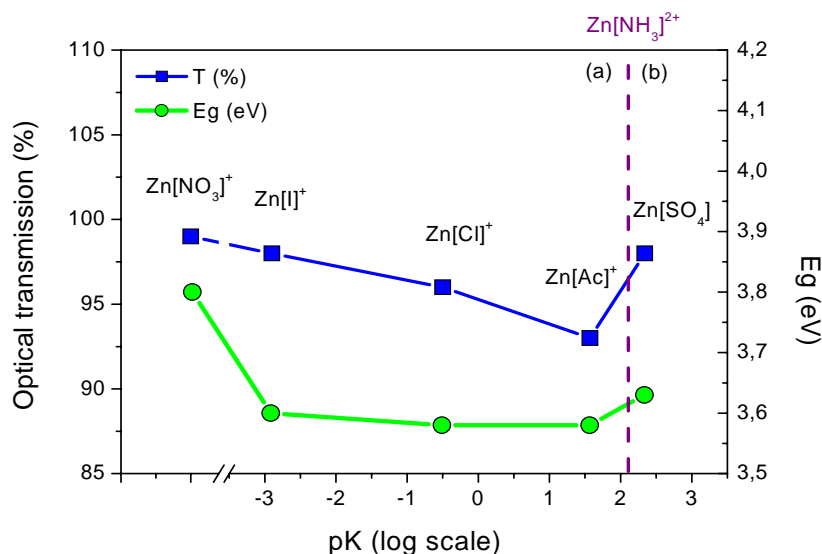
Figure 3.16. Optical transmission (blue squares) and band gap values (green circles) of ZnS(O,OH) films versus the pK of the Zn complex. The dashed line indicates $Zn[NH_3]^{2+}$ complex line

The values of the optical band gap energy were calculated as given in section 2.3.1, the results are shown in Figure 3.16 and Table 3.7. The band gaps of ZnS(O,OH) are in the range of 3.6 eV, except 3.8 eV for the ZnS(O,OH) deposited

from $Zn(NO_3)_2$. Similar results are described in [113] where higher band gap values (3.75-3.93 eV) were gained for CBD-ZnS films deposited from $Zn(NO_3)_2$ in comparison with those from $ZnCl_2$ (3.66 – 3.78 eV) [113]. The results could be explained with differences in crystal structure of the ZnS films from $Zn(NO_3)_2$ and $ZnCl_2$, since hexagonal ZnS has a larger band gap (3.67 eV [37], 3.74 eV [114],) than cubic ZnS (3.54 eV [37] and 3.66 eV[114]).

Electrical properties of ZnS(O,OH) films

Two probe measurements showed that all the deposited ZnS(O,OH) films had electrical resistance higher than 10^9 Ohm.

The results of Kelvin probe measurements are provided in Table 3.7. The values of the work function of ZnS(O,OH) layers from $ZnCl_2$ and ZnI_2 (4.1 eV) were found 0.3 eV lower than the values of the work function of the other ZnS(O,OH) films (4.4 eV). The counter stabilisation time (time spent from the beginning of the measurement until the stabilisation of the value of work function) in the Kelvin probe method was used to characterise electrical properties of ZnS(O,OH) films since fast counter stabilisation speed is an indication of high conductivity of the material. The longer the stabilisation lasts, the higher is the resistivity of the material. In Table 3.7 the stabilisation time of Kelvin probe measurement of different ZnS(O,OH) films is given and the relative resistivity of layers is described by this. The results show relatively high resistivity for ZnS(O,OH) films from ZnI_2 and $Zn(NO_3)_2$, – for the films that contain a remarkable amount of impurities as it was found by XPS measurements. It should be mentioned that the purity (98.5 % in Table 2.1) of the used ZnI_2 and $Zn(NO_3)_2$ precursor salts was slightly lower than the purities of the other used Zn compounds. Combining the results of the Kelvin probe and optical measurements Fermi levels were calculated for the ZnS(O,OH) films as described in section 2.3.2. All ZnS(O,OH) films have *n*-type conductivity while the films deposited from ZnI_2 and $ZnCl_2$ have the highest *n*-type conductivity.

Table 3.7. Kelvin probe and optical band gap measurement results of ZnS films from different zinc sources

Zn source	Work function (eV)	Counter stabilisation time (min)	Relative resistivity	Band gap (eV)	Fermi level (eV)
$Zn(NO_3)_2$	4.4	16	High	3.80	3.30
ZnI_2	4.1	12	High	3.60	3.40
$ZnCl_2$	4.1	2	Low	3.58	3.38
$Zn(Ac)_2$	4.4	6	Average	3.58	3.08
$ZnSO_4$	4.4	3	Low	3.63	3.13

To generalise, it can be stated that three main factors were found that influence the ZnS(O,OH) films properties:

- The study of the anion effect of the used Zn sources of the chemically deposited ZnS(O,OH) film revealed that the growth rate, composition and optical transmission of the ZnS(O,OH) layer depend on the stability of Zn-complex in chemical bath solution. The growth rate of the ZnS film and the ZnS concentration in films increased with the increasing value of Zn precursor's instability constant up to the $Zn[NH_3]^{2+}$ complex line, but decreased dramatically after the line. For the optical transmission the increasing value of Zn precursor's pK showed an opposite effect.
- The band gap value of ZnS(O,OH) films from zinc nitrate 3.8 eV was higher than the band gap value of ZnS(O,OH) films from the other sources (3.6 eV).
- Usage of precursor Zn salts containing donor-type impurities for ZnS(O,OH) (ZnI_2 and $ZnCl_2$) resulted in ZnS(O,OH) films with higher *n*-type conductivity in comparison with the films from other salts. The lower purity (98.5 %) of the used precursor Zn salts was the reason of higher impurity content in the produced films.

3.2.3 CBD-ZnS(O,OH) as a buffer layer in comparison with CdS
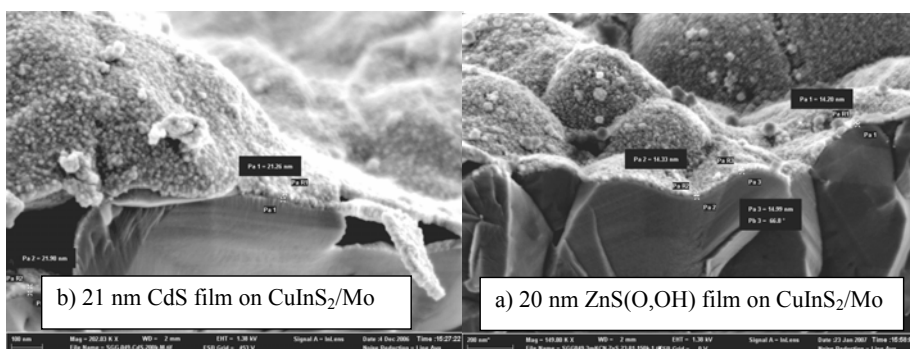
Figure 3.17. SEM micro photos of: (a) ZnS(O,OH) and (b) CdS thin films on CuInS$_2$/Mo

If we compare SEM micro photos of ZnS(O,OH) and CdS thin films grown on CIS, then CdS film morphology deposited from cadmium acetate is quite similar to the ZnS deposited from zinc acetate (Fig. 3.17).

Table 3.8. Thickness and optical properties of some ZnS(O,OH) and CdS films

Buffer layer:anion	Heater temperature (°C)	Film thickness (nm)	Band gap (eV)	Optical transmission (%)
CBD-ZnS:Ac	85	82	3.58	93.3
CBD-ZnS:SO$_4$	85	33	3.63	98.3
CBD-CdS:Ac	55	79	2.30	91.1

If we compare the values of the optical parameters of the buffer layers presented in Table 3.8, we can see that ZnS(O,OH) have higher optical transmission and larger band gap than CdS (Fig. 3.18). Higher transmission is preferable, since more photons will pass the buffer layer and reach the absorber layer.

To conclude, it can be stated that chemically deposited ZnS(O,OH) with the measured higher optical transmission and larger band gap is a good candidate to replace CdS as a buffer layer.
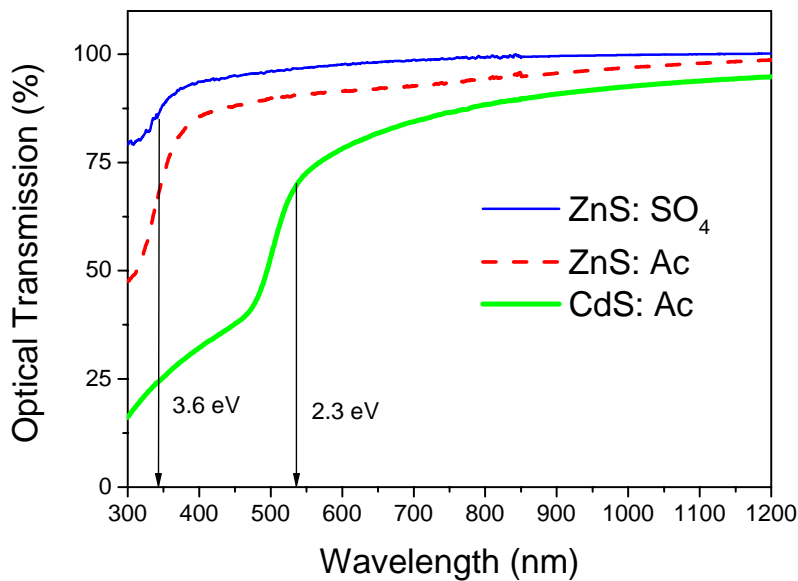
Figure 3.18. Optical transmission curves of ZnS(O,OH) and CdS films on SLG

3.2.4 Results of CISSe and CZTSSe MGL solar cell measurements

Higher transmission is preferable since more photons will pass the buffer layer and reach the absorber layer and result in higher current densities of solar cells. On the other hand, the band gap of ZnS(O,OH) can be too high to suit well with CISSe and CZTSSe. It is well known that too high band gap of ZnS(O,OH) can have a negative effect on solar cell efficiency if too high spike in the *p-n* junction limits the current of the solar cell [32].

Characterisation of CISSe MGL solar cells

The results of spectral response (SR) measurements did not show significant changes for CISSe MGL solar cells with ZnS(O,OH) buffer layers deposited from different zinc sources.

When comparing the spectral responses of CISSe MGL solar cells with ZnS(O,OH) and CdS, we can see that solar cells with ZnS(O,OH) absorb more light in short wavelength region (Fig. 3.19).

Figure 3.19. Results of the spectral response measurements for ZnS(O,OH)/ CISSe (blue line) and CdS/CISSe (red line) MGL solar cells. The dotted lines of the band gaps of different materials are presented

Table 3.9. I-V measurement data for CuIn(S,Se)$_2$ MGL solar cells prepared with different buffer layers

Buffer	V_{OC} (mV)	FF (%)	j_{SC} (mA/cm^2)	η (%)
no buffer	419	43.3	19.4	3.2
CdS:Ac	457	43.3	19.6	3.9
ZnS:SO$_4$	428	46.6	22.7	4.5
ZnS:Ac	439	48.5	23.6	5.0
ZnS:Cl	450	51.2	21.0	4.9
ZnS:I	417	50.5	16.3	3.4
ZnS:NO$_3$	442	50.2	19.6	4.4

Solar cell characteristics gained from I-V measurements (calculations see in section 2.3.3) are given in Table 3.9 for CuIn(S,Se)$_2$ MGL solar cells with no buffer layer, with CdS buffer layers and with ZnS(O,OH) buffer layers. The results show that the chosen zinc source for the deposition of ZnS(O,OH) buffer layers has a major impact on all solar cell parameters. While CdS improved only open-circuit voltage (V_{OC}), the ZnS(O,OH) buffer improved fill factors (FF) in all cases, in comparison with MGL solar cells without any buffer layer. The use of ZnCl$_2$

improved mostly V_{OC} and FF of the solar cells, but the highest MGL solar cell current density (j_{SC}) and as a consequence also the solar cell efficiency (η) was achieved if $Zn(Ac)_2$ was used as a zinc source in the chemical bath deposition solution. Surprisingly, the values of V_{OC} and j_{SC} of $CuIn(S,Se)_2$ MGL solar cells with ZnS(O,OH) prepared from ZnI_2 containing solutions are even lower than those of the solar cells without any buffer layer. This can be due to the higher ZnS(O,OH) resistance resulting from impurity contamination in the ZnS(O,OH) films (see 1.5.1).

Characteristics of CZTSSe MGL solar cells
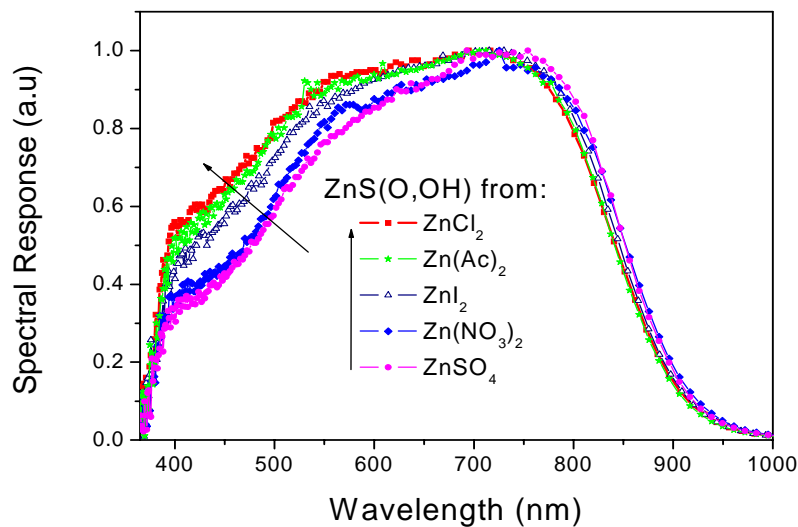
Figure 3.20. Spectral response of ZnS(O,OH)/CZTSSe MGL solar cells, the dependence of the zinc precursors of ZnS(O,OH) on the spectral response

The results of the spectral response measurements for CZTSSe MGL solar cells with ZnS(O,OH) from chemical bath with different zinc salts as zinc sources show remarkable differences in the short wavelength region, as seen in Figure 3.20. The spectral response was the strongest for the CZTSSe MGL solar cells with the ZnS(O,OH) buffer layer deposited from $ZnCl_2$ and $ZnAc_2$ compounds. The weakest response was for the CZTSSe MGL solar cells with the ZnS(O,OH) buffer layer deposited from $Zn(NO_3)_2$ and $ZnSO_4$ salts. The spectral response of the ZnS(O,OH)/CZTSSe MGL solar cells followed the same tendency as in ZnS(O,OH) thickness measurements: spectral response increased with buffer layer thickness in the solar cells in the short wavelength region. The phenomena can be explained with a better shunt blocking action of thicker buffer layers.
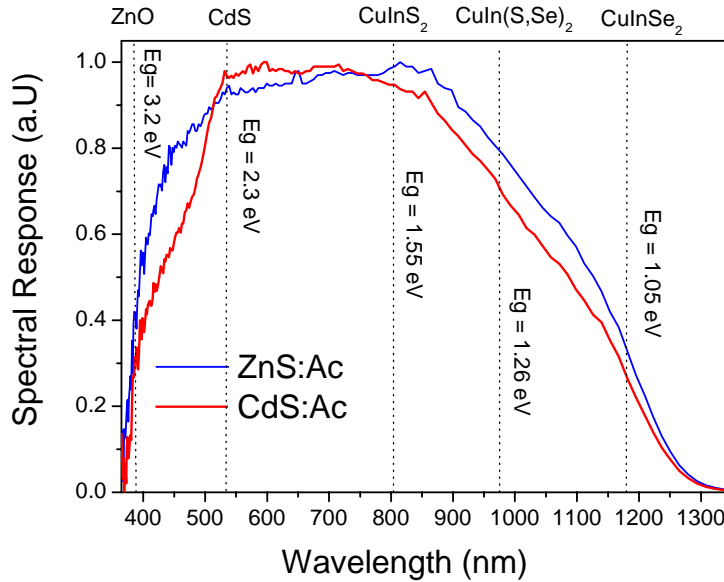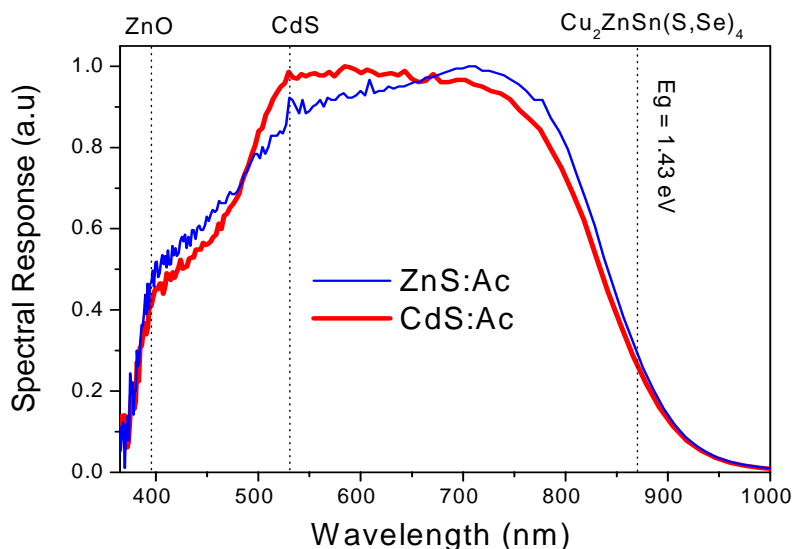
Figure 3.21. The results of spectral response measurements for ZnS(O,OH)/CZTSSe (blue line) and CdS/CISSe (red line) MGL solar cells. The dotted lines mark the band gaps of different materials

If we compare the spectral responses of CZTSSe MGL solar cells with ZnS(O,OH) and CdS, we can see that solar cells with ZnS(O,OH) absorb slightly more photons in the short wavelength region (Fig. 3.21). This is due to the higher band gap energy of the ZnS(O,OH) over CdS, but the effect is not so strong as in the case of CISSe MGL solar cells.

Solar cell characteristics gained from I-V measurements are given in Table 3.10 for $Cu_2ZnSn(S,Se)_4$ MGL solar cells with CdS and ZnS(O,OH) buffer layers. The solar cell with CdS resulted in much higher fill factors than those of ZnS(O,OH)/CZTSSe MGL solar cells.

Table 3.10. I-V measurement data for $Cu_2ZnSn(S,Se)_4$ MGL solar cells prepared with ZnS(O,OH) buffer layers from different zinc precursors

Buffer	V_{OC} (mV)	FF (%)	j_{SC} (mA/cm^2)	η (%)
CdS:Ac	503	53.0	13.2	3.5
ZnS:SO$_4$	503	38.5	11.9	2.3
ZnS:Ac	476	38.1	15.6	2.7
ZnS:Cl	512	38.8	12.6	2.3
ZnS:I	475	31.0	6.4	0.8
ZnS:NO$_3$	465	36.5	8.6	1.1

The impact of the chosen zinc source for the deposition of ZnS(O,OH) buffer layers was studied and it is obvious that it has an influence on all solar cell parameters. The major negative effect is seen in the values of *FF* and j_{SC} of

ZnS(O,OH)/CZTSSe MGL solar cells made using ZnI_2 and $Zn(NO_3)_2$ as a zinc source, probably due to the higher content of impurities in the films.

Anion effect of the zinc precursor on CISSe and CZTSSe MGL solar cells

The values of open circuit voltages and fill factors were only very slightly affected by the variation of the ZnS(O,OH) deposition precursor. The current densities of solar cells increase with the increasing pK values for the Zn[L] and drop after the $Zn[NH_3]^{2+}$ complex line (Fig. 3.22). Figure 3.22 shows that the CISSe and CZTSSe MGL solar cells with ZnS(O,OH) films from ZnI_2 with relatively high resistivity and high impurity content in the films (see Table 3.7 and Fig. 3.15) have the lowest current densities. The curves of solar cell efficiency follow the shape of current density curves (Fig. 3.22). The dependence can be caused by differences in the thickness of ZnS(O,OH) films and the content of ZnS and impurities in the films. The only exceptions are solar cells with ZnS(O,OH) from $Zn(NO_3)_2$ that have the highest transmission and the largest band gap.
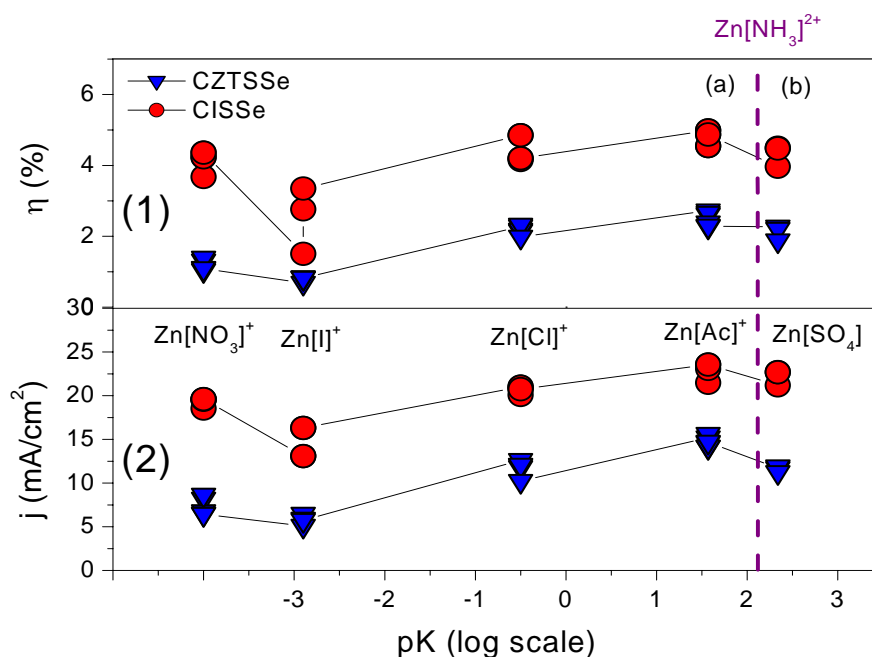
Figure 3.22. Efficiencies (1) and current densities (2) of CISSe (circles) and CZTSSe (triangles) MGL solar cells versus Zn-complex pK values from various zinc precursors. The dashed line indicates $Zn[NH_3]^{2+}$ complex line, which divides the graph into two regions: (a) $pK_{Zn(NH3)2+} > pK_{Zn(L)n}$ and (b) $pK_{Zn(NH3)2+} < pK_{Zn(L)n}$

To summarise the results of our solar cell research, it can be stated that spectral response is higher for solar cells with the ZnS(O,OH) buffer layer in the short wavelength region than with the CdS buffer layer, the effect is more visible in ZnS(O,OH)/CISSe MGL solar cells and less in ZnS(O,OH)/CZTSSe MGL solar cells.

Spectral response of ZnS(O,OH)/CZTSSe MGL solar cells is increasing with the buffer layer thickness in the short wavelength region, no changes were found for ZnS(O,OH)/CISSe MGL solar cells probably due to the well known fact that in CISSe solar cells a buried homojunction forms and it hides the minor influences from different buffer materials properties [42, 115].

An analogous effect of chemical nature of an anion on the growth rate and the ZnS concentration in ZnS(O,OH) films was detected for solar cell current densities and efficiencies. The highest solar cell current densities and efficiencies were achieved with ZnS(O,OH) buffer layers with the highest growth rate and ZnS content deposited from $Zn(Ac)_2$. The only exception was a solar cell with ZnS(O,OH) deposited from $Zn(NO_3)_2$ containing bath that results in ZnS(O,OH) with the widest band gap (3.8 eV) and the highest transmission. The impurities in the ZnS(O,OH) films affect also the $CuIn(S,Se)_2$ and $Cu_2ZnSn(S,Se)_4$ solar cell efficiency by lowering the values of current densities.

3.2.5 Summary of experimental results of the CBD ZnS(O,OH) study

The idea that anions from different zinc salts as Zn sources in a chemical solution for ZnS(O,OH) deposition can act as complexing agents and influence the deposition process was supported by experimental findings.

- The study on the anion effect of the Zn source for the chemical deposition of ZnS(O,OH) films revealed that the growth rate and composition of the ZnS(O,OH) layer depended on the instability constant value of Zn-complex in chemical bath solution. The ZnS(O,OH) film's growth rate and ZnS concentration in films increased with the increasing of the value of Zn precursor's pK up to the $Zn[NH_3]^{2+}$ complex pK value and decreased then.
- All ZnS(O,OH) films had *n*-type conductivity, which was the highest for the ZnS(O,OH) films deposited from ZnI_2 and $ZnCl_2$. ZnS(O,OH) films from ZnI_2 and $Zn(NO_3)_2$ precursors had higher relative resistivity than other ZnS(O,OH) films due to the higher content of impurities in the precursor salt.
- Band gap values of ZnS(O,OH) films being around 3.6 eV did not depend on Zn precursor's instability constant. The only exception was the ZnS(O,OH) film from zinc nitrate with E_g=3.8 eV.
- Chemically deposited ZnS(O,OH) films showed higher optical transmission than CdS.
- Spectral response was found higher for solar cells with ZnS(O,OH) buffer layer in the short wavelength region as compared with the CdS buffer layer, the

effect is more visible in ZnS(O,OH)/CISSe MGL solar cells and less in ZnS(O,OH)/CZTSSe MGL solar cells.

- Spectral response of ZnS(O,OH)/CZTSSe MGL solar cells is increasing with buffer layer thickness in the short wavelength region, no change was found for ZnS(O,OH)/CISSe MGL solar cells probably due to the well known fact that in CISSe solar cells a buried homojunction forms and it hides the minor influence from different buffer materials properties.

- An analogous effect of chemical nature of the anion on the growth rate and the ZnS concentration in ZnS(O,OH) films was detected for solar cell current densities and efficiencies. The only exception was the solar cell with ZnS(O,OH) deposited from $Zn(NO_3)_2$ containing bath that resulted in ZnS(O,OH) with the widest band gap (3.8) eV and the highest transmission.

- The impurities in the ZnS(O,OH) films originating from ZnI_2 and $Zn(NO_3)_2$ salts affect also the $CuIn(S,Se)_2$ and $Cu_2ZnSn(S,Se)_4$ solar cell efficiency by lowering the values of current densities.

- The highest solar cell current densities and efficiencies of CISSe and CZTSSe solar cells were achieved with ZnS(O,OH) buffer layers with the highest growth rate and with the highest ZnS content deposited from $Zn(Ac)_2$ containing solution.

- CISSe MGL solar cells with CBD-ZnS worked more efficiently (η = 5.0 %) than the reference cell with CdS buffer layer (η = 3.9 %) that had lower fill factors and current densities.

- ZnS/CZTSSe MGL solar cells showed solar cell efficiencies up to 2.7 %, while reference solar cells with the CdS buffer layer worked with 3.5 % efficiency, mainly due to higher fill factors.

CONCLUSIONS

The study of different buffer layer materials deposited by two chemical deposition methods to the substitute CdS buffer layer in $CuInSe_2$-type solar cells led to the following conclusions:

USP-In$_2$S$_3$

- USP is a suitable method for growing thin In_2S_3 films with dominating tetragonal phase and with Eg values of 2.6 to 2.9 eV in the range of substrate temperatures of 200 – 245 ºC from alcoholic solutions with a of precursors concentration ratio [TU]:[InCl$_3$] of 2 to 6. The growth rate of oxygen free In_2S_3 films increases with increasing substrate temperature and with precursor concentrations in solution. In comparison with CBD-CdS, the optical properties of USP-In_2S_3 are more suitable for the buffer in $Cu(In,Ga)Se_2$ solar cells.
- CIGSe solar cells with USP-In_2S_3 buffer-layers show efficiencies of up to 9.5 %, lagging behind the reference cells with CBD-CdS buffer-layers with it's 12.7 %. Further studies should optimise the spray conditions for improvement of *p-n* junction formation.

CBD-ZnS

1. It was found that anions from different zinc salts as Zn-sources in chemical bath solution act as complexing agents and influence the ZnS deposition process and the properties of deposited ZnS films as well as the characteristics of solar cells with chemically deposited ZnS buffer layers.
- The study on the anion effect of different Zn sources on the chemical deposition of ZnS(O,OH) films revealed that the growth rate and composition of the ZnS(O,OH) layer depends on the instability constant value of the Zn-complex formed in the chemical bath solution. The ZnS(O,OH) film's growth rate and ZnS concentration in films increases with the value of the Zn complex pK up to the value of the $Zn[NH_3]^{2+}$ complex pK line and decreases after the line.
- The band gap values (around 3.6 eV) of deposited *n-type* ZnS(O,OH) films does not depend on the Zn precursor's instability constant.
- Current densities and efficiencies of CISSe and CZTSSe MGL solar cells increase with the increasing pK values of different zinc complexes for ZnS buffer layers up to the $Zn[NH_3]^{2+}$ complex line and decreased after the line. The highest current densities and efficiencies of CISSe and CZTSSe MGL solar cells were achieved with ZnS(O,OH) buffer layers from zinc acetate containing solution.

2. Due to the higher optical transmission it was found that chemically deposited ZnS(O,OH) is a good candidate to replace CdS. CISSe MGL solar cells with CBD-ZnS worked more efficiently (η = 5.0 %) in comparison with the reference cell with CdS buffer layer (η = 3.9 %). The *p-n* junction formation of ZnS(O,OH) with CZTSSe needs an in depth study.

ABSTRACT

Study of In$_2$S$_3$ and ZnS thin films deposition by ultrasonic spray pyrolysis and chemical deposition

This thesis is focused on studies of ultrasonic spray pyrolysis deposition of In$_2$S$_3$ thin films and chemical bath deposition of ZnS thin films as alternative buffer layers to CBD-CdS for CuInSe$_2$ type absorber materials in PV solar cells.

The first part of the study describes the process of replacing CBD CdS buffer layers in Cu(In,Ga)Se$_2$ solar cells by In$_2$S$_3$ thin film buffer layers deposited by an ultrasonic spray pyrolysis method. USP-In$_2$S$_3$ films were prepared at various substrate temperatures (200, 220 and 245 C) and spray solution concentrations. Thin USP-In$_2$S$_3$ films properties were studied with several techniques including profilometer, spectro-photometer, XPS, XRD, and SEM. USP-In$_2$S$_3$/CIGSe solar cells were studied by measuring their I-V characteristics and by EQE measurements.

The growth rate of the In$_2$S$_3$ film was studied and it was found to increase with increasing substrate temperature and precursor concentrations in the solution. Optical transmission of deposited layers decreased with higher substrate temperature and lower thiourea concentration in the spray solution. SEM images showed that continuous thin In$_2$S$_3$ buffer-layers had been grown on the glass substrates. XRD and XPS measurements revealed that mainly the β-In$_2$S$_3$ phase was formed in the films. The direct optical band gap of *n*-type USP-In$_2$S$_3$ films was found to be around 2.8 eV, while the band gap of CdS was 2.4 eV. The higher band gap and optical transmission of In$_2$S$_3$ in comparison with CdS shows that the optical properties of In$_2$S$_3$ films are suitable for the buffer layer material.

A solar cell efficiency of 9.5 % for In$_2$S$_3$/CIGSe cells was achieved after light soaking if USP-In$_2$S$_3$ was deposited at 220 ºC for 20 minutes from an alcoholic solution containing 0.005 M InCl$_3$ and 0.015 M TU, as compared to 12.9 % efficiency for the reference CIGSe cell with a standard CBD-CdS buffer layer. Current densities of the solar cells were comparable, but lower values of the fill factor and open-circuit voltage led to the problems in the interface between ZnO, In$_2$S$_3$ and CIGS, which was confirmed by SEM, *Voc-T* dependance measurements and the light soaking effect.

The second part of the study is related to CBD-ZnS, which is often containing ZnO and ZnOH and is therefore denoted by ZnS(O,OH). Thin ZnS(O,OH) films were prepared by CBD using Zn(CH$_3$COO)$_2$, ZnCl$_2$, ZnI$_2$, Zn(NO$_3$)$_2$ and ZnSO$_4$ as different zinc sources on SLG, Mo, CISSe monograins and CZTSSe monograins. Different techniques, such as SEM, XPS, XRD, spectro-photometry, Kelvin probe measurements, were used to study thin ZnS(O,OH) film properties.

The growth rate of ZnS(O,OH) films and the ZnS content in films were found to depend on the instability constants of Zn-ligand complexes increasing with the

increasing value of Zn precursor's instability constant up to the $Zn[NH_3]^{2+}$ complex instability constant line and decreased after the line.

Current densities and efficiencies of ZnS(O,OH)/CISSe and ZnS(O,OH)/CZTSSe monograin layer solar cells changed with the instability constants of Zn-ligand complexes formed in chemical bath analogeously to the growth rate of ZnS(O,OH) films. The maximum efficiency of CISSe and CZTSSe monograin layer solar cells was gained using $Zn(CH_3COO)_2$ as the Zn source.

As a result, CISSe solar cells with CBD-ZnS showed 5.0 % solar cell efficiency, when the reference solar cells with CdS buffer layer worked with the efficiency of 3.9 %, having lower values of the fill factor and current density. ZnS/CZTSSe solar cells worked with efficiencies of up to 2.7 %, while reference solar cells with the CdS buffer layer showed the efficiency of 3.5 %, mainly due to higher values of fill factors. The reason is that the real working *p-n* junction in CISSe solar cells is formed on the surface of CISSe, therefore buffer layer's role is mainly optical and structural compatibility. In the case of CZTSSe material, the role of the buffer layer is more critical and the formation of the *p-n* junction forms in the interface of the buffer and absorber material and CdS is more suitable than ZnS(O,OH) for the CZTSSe absorber used in this study.

KOKKUVÕTE

Ultraheli pihustuspürolüüsi ja keemilise sadestamise meetodil kasvatatud In_2S_3 ja ZnS õhukeste kilede uurimine

Käesolevas doktoritöös on uuritud võimalusi asendada $CuInSe_2$ tüüpi ühendpooljuht-päikesepatareides kasutatav CdS puhverkiht vähem tervisele ohtlike ühendite ZnS ja In_2S_3 keemiliselt ja ultraheli pihustuspürolüüsi meetodil kasvatatud kiledega.

Doktoritöö esimese poole eesmärgiks oli leida sobivate omadustega ultraheliliselt pihustatud In_2S_3 õhukene kile, mis asendaks keemiliselt sadestatud CdS puhverkihi $Cu(In,Ga)Se_2$ päikesepatareides. Selleks uuriti In_2S_3 kilede kasvu erinevatel sadestustemperatuuridel (200, 220 and 245 ˚C) ja ja sadestatud kilede omadusi erinevatel pihustuslahuste kontsentratsioonidel. Õhukeste In_2S_3 kilede omaduste uurimiseks kasutati erinevaid meetodeid nagu profilomeetria, spektrofotomeetria, XPS, XRD ja SEM. Erinevatel tingimustel sadestatud puhverkihtidega CIGSe päikesepatareide omadusi uuriti volt-amper karakteristikute ja kvantefektiivsuse mõõtmiste teel.

Leiti, et In_2S_3 kile kasvukiirus suureneb aluskihi temperatuuri ja lähtesoolade kontsentratsiooni suurendamisel pihustuslahuses. Kilede läbipaistvus väheneb aluskihi temperatuuri suurendamisel ja tiokarbamiidi vähendamisel pihustuslahuses. Skaneeriva elektronmikroskoobi (SEM) kujutistel võis näha, et klaasile kasvasid pidevad ja õhukesed In_2S_3 kiled. XRD ja XPS mõõtmised näitasid, et kiled sisaldasid peamiselt *β*-In_2S_3 faasi, mille keelutsooni laiuseks saadi 2.8 eV (CdS keelutsooni laius on 2.4 eV). CdS-st suurem keelutsooni laius ja läbipaistvus näitavad, et *β*-In_2S_3 õhukeste kilede optilised omadused on sobivad puhverkihi jaoks.

In_2S_3/CIGSe päikesepatareide kasuteguriks mõõdeti 9,5 % samal ajal kui võrdlusobjekti CdS/CIGSe päikesepatarei kasuteguriks mõõdeti 12.9 %. Päikesepatareis kasutatud In_2S_3 kile kasvatati 0.005 M $InCl_3$ ja 0.015 M TU sisaldavast metanooli lahusest 220 ºC juures, kestvusega 20 minutit. Päikesepatareide voolutihedused olid võrdsed, kuid In_2S_3-ga päikesepatarei madalamad täituvusastmed (*FF)* ja avatud ahela pinged viitasid kontaktprobleemidele ZnO, In_2S_3 ja CIGS materjalide siirdealadel, mis leidis kinnitust ka objektide uurimisel skaneeriva elektronmikroskoobiga ja avatud ahela pinge temperatuursõltuvuse mõõtmisega.

Kokkuvõtteks võib öelda, et töös leiti sobivad tingimused In_2S_3 kilede sadestamiseks ultraheli pihustuspürolüüsi meetodil ja et sadestatud In_2S_3 kiled sobivad CIGSe tüüpi päikesepatareidesse puhverkihiks, kuid probleemid siirdealal vajavad veel edasist uurimist.

Doktoritöö teises osas uuriti keemilises vannis sadestatud ZnS õhukesi kilesid, mis tingituna sagedase ZnO ja $Zn(OH)_2$ kaasasadenemisega, kirjutatakse tihti kujul

ZnS(O,OH). Õhukesed ZnS(O,OH) kiled sadestati erinevatele alusmaterjalidele: klaasile, molübdeenile ja erinevatele absorbermaterjalidele – CISSe ning CZTSSe monoteradele. Uurimistöö põhitähelepanu oli suunatud erinevate sadestuslahuses kasutatavate tsingisoolade mõjule nii sadestusprotsessile kui ka sadestatud kilede omadustele. Selleks varieeriti tsingi allikaid sadestuslahuses: $(Zn(CH_3COO)_2$, $ZnCl_2$, ZnI_2, $Zn(NO_3)_2$ ja $ZnSO_4$. Kilede omaduste uurimiseks kasutati erinevaid meetodeid: SEM, XPS, XRD, spektrofotomeetriat ja Kelvin sondi meetodit.

Töös leiti, et ZnS(O,OH) kiled paksus ja ZnS sisaldus kiledes sõltusid Zn-soola kompleksi ebapüsivuskonstandi tugevusest alljärgnevalt: kilede paksused ja ZnS sisaldus kiledes suurenesid ebapüsivuskonstandi suurenemisel kuni $Zn[NH_3]^{2+}$ kompleksi vastava väärtuseni ja vähenesid peale seda.

Kõik sadestatud ZnS(O,OH) kiled olid n-tüüpi juhtivusega, suurema läbipaistvusega ja keelutsooni laiusega võrreldes CdS kiledega, seetõttu on nad sobivad kandidaadid puhverkihiks. ZnS(O,OH) keelutsooni laiuseks mõõdeti 3.6 eV, välja arvatud 3.8 eV kiledele, mis sadestati kasutades $Zn(NO_3)_2$ soola. Kelvin sondi mõõtmised näitasid, et ZnS(O,OH) kiled, mis sisaldasid XPS mõõtmiste järgi lisandeid ning kasvatati väiksema puhtusega sooladest (98.5 % ZnI_2 ja $Zn(NO_3)_2$ puhul), olid suurema takistusega.

ZnS/CISSe ja ZnS/CZTSSe monotera-päikesepatareide voolutihedused ja efektiivsused järgisid samaseid muutusi sõltuvalt kasutatud Zn-sooladest kui ZnS(O,OH) kilede paksused ja ZnS sisaldus kiledes. Erandiks oli suurema keelutsooni laiuse ja läbipaistvusega $Zn(NO_3)_2$-st sadestatud ZnS(O,OH) puhverkiht, mis võimaldas päikesepatareil absorbeerida rohkem valguskiirgust. Suurimad kasutegurid mõõdeti CISSe ja CZTSSe päikesepatareidele, mille ZnS(O,OH) puhverkiht oli sadestatud lahusest, kus tsingi allikana oli sadestatud tsinkatsetaati.

ZnS/CISSe monotera päikesepatareide kasuteguriks mõõdeti 5,0 %, samal ajal kui võrdluseks valmistatud CdS/CISSe monotera-päikesepatareide kasuteguriks mõõdeti 3,9 %, seda peamiselt väiksema täituvusastme ja voolutiheduse tõttu. ZnS/CZTSSe monotera- päikesepatareide maksimaalseks efektiivsuseks mõõdeti 2.7 %, võrdluseks valmistatud CdS/CZTSSe päikesepatarei efektiivsuseks mõõdeti 3.5 %, eelkõige suurema täituvusastme tõttu. Puhverkihi roll CZTSSe monotera-päikesepatareides vajab edasist uurimist.

Kokkuvõtvalt võib öelda, et töös leitud sadestustingimustel keemilises vannis sadestatud ZnS(O,OH) sobib asendama CdS puhverkihti $CuIn(S,Se)_2$ päikesepatareides. $Cu_2ZnSn(S,Se)_4$ päikesepatareide puhul vajab p-n ülemineku moodustumine veel põhjalikumat uurimistööd.

REFERENCES

1. T. Asikainen, M. Ritala and M. Leskela. Appl. Surf. Sci. 82 (1994) 122
2. N. Naghavi, S. Spiering, M. Powalla, B. Cavana, D. Lincot. Prog. Photovolt. Res. Appl 11 (2003) 437.
3. N. Barreau, S. Narsillac, D. Albertini, J.C. Bernede. Thin Solid Films 403-404 (2002) 331.
4. O. Madelung, Semiconductors Other than Group IV Elements and III-V Compounds, Springer, Berlin (1992) 26.
5. M. Bredol, J. Merikhi. J. Mater. Sci. 33 (1998) 471–476.
6. A.U. Ubale, D.K. Kulkarni. Bull. Mater. Sci. 28 (1) (2005) 34–47.
7. F. Zhenyi, C. Yichao, H. Yongliang, Y. Yaoyuan, D. Yanping, Y. Zewn, T. Hongchang, Y. Hogfao, W. Heming, J. Cryst. Growth 237–239 (2002) 1707–1710.
8. M. Ichimura, F. Gato, Y. Ono, E. Arai, J. Cryst. Growth 198–199 (1999) 308–312.
9. S. Lindroos, Y. Chrreire, D. Bonnin, M. Leskela, Mater. Res. Bull. 33 (3) (1998) 453–459.
10. H.H. Afifi, S.A. Mohmoud, A. Ashour, Thin Solid Films 263 (1995) 248–251.
11. R. Nomura,T. Murai,T.Toyosaki, H. Matsuda, Thin Solid Films 271 (1995) 4–7.
12. A.M. Chaparro, C. Maffiotte, M.T. Gutierrez, J. Herrero, Thin Solid Films 358 (2000) 22–29.
13. P. Roy, J.R. Ota, S.K. Srivastava, Thin Solid Films 515 (2006) 1912–1917.
14. M. Lodar, E.J. Popovici, I. Baldea, R. Grecu, E. Indrea, J. Alloys Compd.434–435 (2007) 697–700.
15. C. Hubert, N. Naghavi, B. Canava, A. Etcheberry, D. Lincot, Thin Solid Films 515 (2007) 6032–6035.
16. F. Gode, C. Gumus, M. Zor, J. Cryst. Growth 299 (2007) 136–141.
17. L.V. Makhova, I. Konovalov, R. Szargan, N. Aschkenov, M. Schubert, T.Chasse, Phys. Stat. Sol. 2 (3) (2005) 1206–1211.
18. W.T. Kim, C.D. Kim, J. Appl. Phys. 60 (1986) 2631.
19. N. Kamoun, S. Belgacem, M. Amlouk, R. Bennaceur, J. Bonnet, F. Touhari, M. Nouaoura, L. Lassabatere, J. Appl. Phys. 89 (2001) 2766.
20. A. A. El Shazly, D. Abd Elhady, H. S. Metwally, M. A. M. Seyam, J. Phys.: Condens. Mater., 10 (1998) 5943.
21. S. H. Choe, T. H. Bang, N. O. Kim, H. G. Kim, C. I. Lee, M. S. Jin, S. K. Oh, W. T. Kim, Semicond. Sci. Technol. 16 (2001) 98.
22. M. Amlouk, M.A. Ben Said, N. Kamoun, S. Belgacem, N. Brunet, D. Barjon, Jpn. J. Appl. Phys 38 (1999) 26.
23. W. Rehwald, G. Harbeke, J. Phys. Chem. Solids 26 (1965) 1309.

24. J.M. Giles, H. Hatwell, G. Offergeld, J. van Cakenberghe, J. Phys. Status Solidi 2 (1962) K73.
25. E. Dalas, S. Sakkopoulos, E. Vitoratos, G. Maroulis, J. Mater. Sci. 28 (1993) 5456
26. R. Baylon, C. Guillen, M.A. Martinez, M.T. Gutierrez, J. Herrero, J. Electrochem. Soc. 145-8 (1998) 2775
27. C.D. Lokhande, A. Ennaoui, P.S. Patil, M. Giersig, K. Diesner, M. Muller, H. Tributsch, Thin Solid Films 340 (1999) 18
28. R.S. Mane, C.D. Lokhande, Materials Chemistry and Physics 78 (2002) 15
29. K. Ernits, Influence of absorber layer chemical treatments on CuInSe2 solar cell parameters, Bachelor thesis (2004) Tallinn University of Technology
30. B. Roedern, G.H. Bauer, Material Requirements for Buffer Layers Used to Obtain Solar Cells with High Open Circuit Voltages. Proceedings of the MRS Spring Meeting1999, 2001
31. H.S. Ullal, Polycrystalline thin film photovoltaic technologies: progress and technical issues, NCPV/NREL, USA (aivalable online)
32. Jim Sites, Chalcogenide Solar Cells: Choosing the Window, EMRS Spring Meeting 2004
33. D. Hariskos, S. Spiering, M. Powalla, Thin Solid Films 480-481 (2005) 99
34. P.K. Nair, M.T.S. Nair, V.M. Carcia, O.L. Arenas, Y. Pena, A. Castillo, I.T. Ayala, O. Gomezdaza, A. Sanchez, J. Campos, H. Hu, R. Suarez, M.E. Rincon, Solar Energy Materials and Solar Cells 52 (1998) 313
35. I. Repins, M.A. Contreras, B. Egaas, C. DeHart, J. Scharf, C.L. Perkins, B. To, R. Noufi, Prog. Photovolt: Res. Appl. 16 (2008) 235
36. K.S. Ramaiah, A.K. Bhatnagar, R.D. Pilkington, A.E. Hill, R.D. Tomlinson, Journal of Materials Science: Materials in Electronics 11 (2000) 267
37. D.R. Lidle, CRC Handbook of Chemistry and Physics, 78th edition, 1997 – 1998, p 12-93
38. G. Hodes, Chemical solution deposition of semiconductor films, Weizmann Institute of Science, Rehovot, Israel, 2003 p. 136
39. L.L. Kazamerski, F.R. White, S. Ayyagari, Y.J. Juang, R.P. Patterson, J. Vac. Sci. Technol. 14 (1977) 65
40. H. Peng, C. Xie, D.T. Schoen, K. Mcllwrath, X.F. Zhang, Y. Cui, Nano Letteters 7:12 (2007) 3734
41. I.-H. Choi, P.Y. Yu, Phys. Stat. Sol. B 242:8 (2005) 1610
42. K. Ernits, Comparison of CdS films deposited from chemical baths containing different donor type impurities and doping effect to $CuInSe_2$/CdS solar cells. Master thesis, Tallinn, 2005 p.13
43. C. Platzer-Björkman, Band Alignment Between ZnO-Based and $Cu(In,Ga)Se_2$ Thin Films for High Efficiency Solar Cells. Dissertation (2006) Uppsala University
44. S.D. Sartale, B.R. Sankapal, M. Lux-Steiner, A. Ennaoui, Thin Solid Films 480 (2005) 168

45. T.T. John, S. Bini, Y. Kashiwaba, T. Abe, Y. Yasuhiro, C.S. Kartha and K.P. Vijayakumar, Semicon. Sci. Technol. 18 (2003) 491

46. I. Puspitasari, T.P. Gujar, K.-D. Jung, O.-S. Joo, Journal of Materials Processing Technology 201 (2008) 775

47. N. Naghavi, R. Henriquez, V. Laptev, D. Lincot, Applied Surface Science 222 (2004) 65

48. M.G. Sandoval-Paz, M. Sotelo-Lerma, J.J. Valenzuela-Jauregui, M. Flores-Acosta, R. Ramirez-Bon, Thin Solid Films 472 (2005) 5

49. M.M. El-Nahass, B.A. Khalifa, H.S. Soliman, M.A.M. Seyam, Thin Solid Films 515 (2006) 1796

50. Wikipedia – online encyclopedia: http//en.wikipedia.org/wiki/Solar_cell#Three_generations_of_solar_cells

51. H.-J. Lewerenz, H. Jungblut, Photovoltaik. Grundlagen und Anwendungen. Berlin, Heidelberg: Springer-Verlag, 1995

52. Homepage of University of Strathclyde: level2.phys.strath.ac.uk/SolarEnergy/

53. M. Kauk, Chemical Composition of $CuInSe_2$ Monograin Powders for Solar Cell Application. Doctoral thesis, Tallinn, TUT (2006)

54. C.H. Champness, Journal of Material Science: Materials in Electronics 10 (1999) 605

55. JCPDS File 27-0159

56. J.L. Hay, B. Tell, H.M. Kasper, L.M. Schiavone, Phys. Rev. B7 (1973) 4485

57. I. Kaiser, K. Ernst, Ch-H. Fisher, Sol. En. Mat. Sol. Cells 67 (2001) 89

58. W.K. Kim, E.A. Payzant, S.S. Li, O.D. Crisalle, T.J. Anderson, IEEE Xplore 1-4244-0016-3 (2006) 453

59. W. Schäfer, R. Nitsche, Mater. Res. Bull. 9 (1974) 645

60. Y.B. Kishore Kumar, G. Suresh Babu, P. Uday Bhaskar, V. Sundara Raja, Sol. En. Mat. Sol. Cells XXX

61. J.J Schragg, P.J. Dale, L.M. Peter, Thin Solid Films 517 (2009) 2481

62. T. Todarov, M. Kita, J. Carda, P. Escribano, Thin Solid Films 517 (2009) 2541

63. K. Timmo, M. Altosaar, J. Raudoja, K. Muska, M. Danilson and T. Varema, (available online: *www.irc.ee/pvconference/download.php?nimi=timmo.pdf*) 3rd Nordic PV Conference 2009.

64. R.A. Wibowo, K.H. Kim, Sol. En. Mat. Sol. Cells XXX

65. H. Matsushita, T. Maeda, A. Katsui, T. Takizawa, J. Cryst. Growth 208 (2000) 416

66. I.D. Olekseyuk, L.D. Gulay, I.V. Dydchak, L.V. Piskach, O.V. Parasyuk, O.V. Marchuk, J. Alloy. Compds. 340 (2002) 141

67. D. Abou-Ras, G. Kostroz, A. Strohm, H.W. Schock, A.N. Tiwari, J. Appl. Phys. 98 (2005) 123512

68. P. O'Brien, D. J. Otway, J.R. Walsh, Thin Solid Films 315 (1998) 57

69. N.A. Allsop, A. Schönmann, H.-J. Muffler, M. Bär, M.C. Lux-Steiner, C.-H. Fischer, Prog. Photovolt: Res. Appl. 13 (2005) 1

70. C.H. Fisher, H.-J. Muffler, M. Bär, T. Kropp, A. Schönmann, S. Fiechter, G. Barbar, M.C. Lux-Steiner, J. Phys. Chem. B 107 (2003) 7516

71. M. Amlouk, M.A. Ben Said, N. Kamoun, S. Belgacem, N. Brunet, D. Barjon, Jpn. J. Appl. Phys. 38 (1999) 26

72. N. Kamoun, R. Bennaceur, M. Amlouk, S. Belgacem, N. Mliki, J.M. Frigerio, M.L. Theye, Phys. Stat. Sol. 169 (1998) 97

73. R.R. Pai, T.T. John, Y. Kashiwaba, T. Abe, K.P. Vijayakumar, C.S. Kartha, Journal of Materials Science 40 (2005) 741

74. L. Bhira, H. Essaidi, S. Belgacem, G. Couturier, J. Salardenne, N. Barreaux, J.C. Bernede, Phys. Stat. Sol. 181 (2000) 427

75. T. Nakanishi, K. Ito, Solar Energy Materials and Solar Cells 35 (1994) 171

76. P. O'Brien, J.McAleese, J. Mater. Chem. 8 (1998) 2309

77. P. O'Brien, J. McAleese, J. Mater. Chem. 8(11) (1998) 2309

78. J.-H. Lee, J.-S. Yi, K.-J. Yang, J.-H. Park, R.-D. Oh, Electrical and optical properties of boron doped CdS thin films prepared by chemical bath deposition, Thin Solid Films 431:344, 2003

79. C.D. Lokhande, S.H. Pawar, Sol. State Commun. 44:1137, 1982

80. A. Ennaoui, M. Bär, J. Klaer, T. Kropp, R. Saez-Araoz, M.C. Lux-Steiner, Proceedings of 20th EPSEC, xxx

81. P. O'Brien, D.J: Otway, D. Smyth-Boyle, Thin Solid Films 361 (2000) 17

82. T. Nakada, M. Mizutani, Y. Hagiwara, A. Kunioka, Solar Energy Materials & Solar cells 67 (2001) 255

83. A. Ennaoui, W. Eisele, M. Lux-Steiner, T.P. Niesen, F. Karg, Thin Solid Films 431 (2003) 335

84. M. Rusu, W. Eisele, R. Würz, A. Ennaoui, M.C. Lux-Steiner, T.P. Niesen, F. Karg, Journal of Physics and Chemistry of Solids 64 (2003) 2037

85. S. Kundu, L.C. Olsen, Thin Solid Films 471 (2005) 298

86. B. Mokili, Y. Charreire, R. Cortes, D. Lincot, Thin Solid Films 288 (1996) 21

87. C.D. Lokhande, H.M. Pathan, M. Giersig, H. Tributsch, Applied Surface Science 187 (2002) 101

88. R.N. Bhattacharya, M.A. Contreras, G. Teeter, Japanese Journal of Applied Physics 43 (2004) L1475

89. T. Nakada, M. Mizutani, Y. Hagiwara, A. Kunioka, Solar Energy Materials & Solar Cells 67 (2001) 255

90. M.A. Contreras, T. Nakada, M. Hongo, A.O. Pudov, J.R. Sites, E.-Proc. 3rd World Conf on Photovoltaic Energy Conversion (2003) 147

91. Zhou Limei, Xue Yuzhi, Li Jianfeng, Journal of Environmental Sciences Supplement (2009) S76

92. J. Lee, S. Lee, S. Cho, S. Kim, I.Y. Park, Y.D. Choi, Materials Chemistry and Physics 77 (2002) 254

93. A. Ennaoui, S. Siebentritt, M.Ch. Lux-Steiner, W. Riedl, F. Karg, Solar Energy Materials & Solar Cells 67 (2001) 31

94. J. Vidal, O. Vigil, O. de Melo, N. Lopez, O. Zelaya-Angel, Materials Chemistry and Physics 61 (1999) 139

95. J. Vidal, O. de Melo, O. Vigil, N. Lopez, G. Contreras-Puente, O. Zelaya-Angel, Thin Solid Films 419 (2002) 118
96. G.A. Kitajev, S.G. Mokrushin, A.A. Uritskaya, Kolloid Zh. 27 (1965) 51
97. R. Ortega-Borges, D. Lincot, J. Electrochem. Soc. 140 (1993) 3464
98. H. Khallaf, I.O. Oladeji, G. Chai, L. Chow, Thin Solid Films 516 (2008) 7306
99. J.J. Loure, Handbook of analythical chemistry, izdatelstvo "Himia" 1965 (in russian: Ю.Ю. Лурье "Справочник по аналической химий", издательство химия 1965)
100. Handbook of chemistry III, izdatelstvo "Himia" 1965 (in russian: "Справочник химика III", издательство химия 1964)Homepage of Chemguide about stability constants of complex metal ions: http://www.chemguide.co.uk/inorganic/complexions/stabconst.html
102. D. Rudmann, D. Brémaud, A.F. da Cunha, G. Bilger, A. Strohm, M. Kaelin, H. Zogg and A.N. Tiwari, Thin Solid Films 480–481 (2005) 55
103. M. Altosaar, A. Jagomägi, M. Kauk, M. Krunks, J. Krustok, E. Mellikov, J. Raudoja, T. Varema, Thin Solid Films 431-432 (2003) 466
104. M. Altosaar, J. Raudoja, K. Timmo, M. Danilson, M. Grossberg, J. Krustok and E. Mellikov, Phys. Stat. Sol (a) 205 (2008) 167
105. E. Mellikov, D. Meissner, T. Varema, M. Altosaar, M. Kauk, O. Volobujeva, J. Raudoja, K. Timmo, M. Danilson, Solar Energy Materials & Solar Cells 93 (2009) 65
106. Landolt-Börnstein – Group III Condensed Matter Vol 41B: "II-VI and I-VII Compounds; Semimagnetic Compounds", 1999
107. M.G. Sandoval-Paz, M. Sotelo-Lerma, J.J. Valenzuela-Jauregui, M. Flores-Acosta, R. Ramirez-Bon, Thin Solid Films 472 (2005) 5
108. T. Gödecke, K. Schubert, Z. Metallkd. 76 (1985) 357
109. K. Kushiya, Solar Energy 77 (2004) 717
110. F.J. Haug, D. Rudmann, H. Zogg, A.N. Tiwari, Thin Solid Films 431 (2003) 431
111. S. Buecheler, D. Corica, D. Guettler, A. Chirila, R. Verma, U. Müller, T.P. Niesen, J. Palm, A.N. Tiwari, Thin Solid Films 517 (2009) 2312
112. Handbook of chemistry II, izdatelstvo "Himia" 1965 p. 252 (in russian: "Справочник химика II", издательство химия 1964)
113. A. Antony, K.V. Murali, R. Manoj, M.K. Jayaraj, Materials Chemistry and Physics 90 (2005) 106
114. Physics of $A^{II}B^{VI}$ compounds, izdatelstvo "Nauka" 1986 p. 291 (in Russian: "Физика соединений $A^{II}B^{VI}$", издательство "Наука" 1986)
115. M. Altosaar, K. Ernits, J. Krustok, T. Varema, J. Raudoja, E. Mellikov, Thin Solid Films 480 (2005) 147

APPENDIX A

Article I

K. Ernits, D. Brémaud, S. Buecheler, C.J. Hibberd, M. Kaelin, G. Khrypunov, U. Müller, E. Mellikov, A.N. Tiwari. Characterisation of ultrasonically sprayed In_xS_y buffer layers for $Cu(In,Ga)Se_2$ solar cells. Thin Solid Films 515 (2007) 6051.

Appendix A

Article II

K. Ernits, M. Kaelin, D. Bremaud, T. Meyer, U. Müller and A.N. Tiwari. Ultrasonically sprayed In_2S_3 films for $Cu(In,Ga)Se_2$ solar cells. Proceedings of 21st EPSEC (2006) p. 1853.

Appendix A

Article III

E. Mellikov, M. Altosaar, M. Krunks, J. Krustok, T. Varema, O. Volobujeva, M. Grossberg, L. Kaupmees, T. Dedova, K. Timmo, K. Ernits, J. Kois, I. Oja Acik, M. Danilson, S. Bereznev. Research in solar cell technologies at Tallinn University of Technology. Thin Solid Films 516 (2008) 7125.

Appendix A

Article IV

K. Ernits, K. Muska, M. Kauk, M. Danilson, J. Raudoja, T. Varema, O. Volobujeva, M. Altosaar. Chemical bath deposition of ZnS films using different Zn-salts. Physics Procedia xx (2009) xxx, *presented in the conference E-MRS 2009*.

Appendix A

Article V

K. Ernits, K. Muska, M. Danilson, J. Raudoja, T. Varema, O. Volobujeva, M. Altosaar. Anion effect of zinc source to chemically deposited ZnS(O,OH) films. Submitted for publishing in Advances in Material Science and Engineering, MS no. 372708.v1.

APPENDIX B

Curriculum Vitae

ELULOOKIRJELDUS

1. Isikuandmed
    Ees- ja perekonnanimi   Kaia Ernits
    Sünniaeg ja -koht   18.09.1978, Rapla, Eesti
    Kodakondsus   Eestlane

2. Kontaktandmed
    Aadress   Akadeemia tee 5a-31, 12611 Tallinn
    Telefon   +3725160819
    E-posti aadress   kaia@staff.ttu.ee

3. Hariduskäik

Õppeasutus	Lõpetamise aeg	Haridus (eriala/kraad)
Tallinna Tehnikaülikool	2009	Doktorikraad loodus- ja täppisteadustes
Tallinna Tehnikaülikool	2005	Loodusteaduste magistri kraad
Tallinna Tehnikaülikool	2004	Loodusteaduste bakalaureuse kraad
Rapla Õppekeskus	1998	Sekretär-raamatupidaja elukutse
Kohila Gümnaasium	1996	Keskharidus

4. Keelteoskus (alg-, kesk- või kõrgtase)

Keel	Tase
Eesti keel	Emakeel, kõrgtase
Inglise keel	Kõrgtase
Saksa keel	Kesktase
Vene keel	Kesktase
Soome keel	Algtase

5. Täiendõpe

Õppimise aeg	Täiendusõppe läbiviija nimetus
21. – 25. august 2006	"Young Scienist summer scool on photovoltaics", Tallinna Tehnikaülikool
18. – 31. juuli 2004	BEST suvekursus „Energy- Wake up, we´re tomorrow!", Leuveni katoliiklik ülikool, Belgia
17. – 21. mai 2004	CEI-Europe kursus „Thin Film Deposition and Applications", Angströmi laboratoorium, Uppsala ülikool, Rootsi

6. Teenistuskäik

Töötamise aeg	Tööandja nimetus	Ametikoht
Alates 01.09.2009	OÜ crystalsol	Vanemteadur
01.09.2006 – 31.08.2009	TTÜ	Teadur
10.04.2005 – 30.09.2006	ETH Zürich	Akadeemiline külaline
01.09.2005 – 31.08.2006	TTÜ	Erakorraline teadur
01.01.2003 – 31.08.2005	TTÜ	Tehniline töötaja

7. Teadustegevus

Aeg	Nimetus	Tegevus
8. – 12. juuni 2009	EMRS Spring Meeting 2009, Strasbourg, Prantsusmaa	Konverentsi assistent; 1 posterettekanne: "Chemical bath deposition of ZnS films using different Zn-salts"
18. – 19. mai 2009	3rd Nordic PV Conference, Tallinn, Eesti	1 suuline ettekanne "Chemical bath deposited ZnS thin films for CuIn(S,Se)$_2$ solar cells"; 1 posterettekanne: "Electrodeposition of thin compound absorbers for solar cells"
4. – 8. september 2006	21st EPVSEC, Dresden, Saksamaa	1 suuline ettekanne: "Ultrasonically Sprayed In$_2$S$_3$ Buffer-Layers for Cu(In,Ga)Se$_2$"
29. mai – 3. juuni 2006	EMRS Spring meeting 2006, Nice, Prantsusmaa	Konverentsi assistent; 3 posterettekannet: "Characterization of Ultrasonically Sprayed In$_x$S$_y$ Buffer-Layers for Cu(In,Ga)Se$_2$ Solar Cells", "Deposition of CuInSe$_2$ layers with a novel process for low cost solar cells", "Flexible Cu(In,Ga)Se$_2$ on Al-Foils and the effects of Al during Chemical Bath Deposition"

8. Kaitstud lõputööd

"CdS legeerimine doonorlisanditega keemilisel sadestamisel ja selle mõju CuInSe$_2$/CdS päikesepatareile", magistritöö, juhendaja vanemteadur Mare Altosaar.
"CuInSe$_2$ absorberkihi keemiliste töötluste mõju päikeseelemendi parameetritele", bakalaureusetöö, juhendaja vanemteadur Mare Altosaar.

9. Teadustöö põhisuunad

Loodusteadused ja tehnika; keemia ja keemiatehnika; pooljuhtmaterjalidest päikesepatarei *p-n* siirde kujundamine; päikese-energeetika materjalid.

CURRICULUM VITAE

1. Personal data
   Name   Kaia Ernits
   Date and place of birth   18.09.1978, Rapla, Eesti
   Nationality   Estonian

2. Contact information
   Address   Akadeemia tee 5a-31, 12611 Tallinn
   Phone   +3725160819
   E-mail   kaia@staff.ttu.ee

3. Education

Educational institution	Graduation year	Education (field of study/degree)
Tallinn University of Technology	2009	Doctoral study, Doctor of Philosophy in Chemistry and Exact Sciences
Tallinn University of Technology	2005	Master study/Master of Science in Natural Sciences
Tallinn University of Technology	2004	Bachelor study/Bachelor of Science in Natural Sciences
Rapla Educational centre	1998	Secretary and bookkeeper profession
Kohila Gymnasium	1996	General education

4. Language competence/skills (fluent, average, basic skills)

Language	Level
Estonian	Fluent, mother tongue
English	Fluent
German	Average
Russian	Average
Finnish	Basic

5. Special courses

Period	Educational or other organisation
August 21 – 25, 2006	"Young Scientist summer school on photovoltaics", Tallinn University of Technology
July 18 – 31, 2004	BEST summer course "Energy- Wake up, we´re tomorrow!", Catholic University of Leuvenl, Belgium
May 17 – 21,	CEI-Europe course "Thin Film Deposition and Applications",

2004	Angström Laboratory, Uppsala University, Sweden

6. Professional employment

Period	Organisation	Position
From 01.09.2009	OÜ crystalsol	Senior scientist
01.09.2006 – 31.08.2009	TUT	Scientist
10.04.2005 – 30.09.2006	ETH Zürich	Academic Guest
01.09.2005 – 31.08.2006	TUT	Exceptional scientist
01.01.2003 – 31.08.2005	TUT	Technical worker

7. Scientific work

Period	Event	Activity
June 8 – 12, 2009	EMRS Spring Meeting 2009, Strasbourg, France	Conference assistant; 1 poster presentation: "Chemical bath deposition of ZnS films using different Zn-salts"
May 18 – 19, 2009	3rd Nordic PV Conference, Tallinn, Estonia	1 oral presentation "Chemical bath deposited ZnS thin films for CuIn(S,Se)$_2$ solar cells"; 1 poster presentation: "Electrodeposition of thin compound absorbers for solar cells"
September 4 – 8, 2006	21st EPVSEC, Dresden, Germany	1 oral presentation: "Ultrasonically Sprayed In$_2$S$_3$ Buffer-Layers for Cu(In,Ga)Se$_2$"
May 29 – June 3, 2006	EMRS Spring meeting 2006, Nice, France	Conference assistant; 3 poster presentation: "Characterization of Ultrasonically Sprayed In$_x$S$_y$ Buffer-Layers for Cu(In,Ga)Se$_2$ Solar Cells", "Deposition of CuInSe$_2$ layers with a novel process for low cost solar cells", "Flexible Cu(In,Ga)Se$_2$ on Al-Foils and the effects of Al during Chemical Bath Deposition"

8. Defended thesis

"Comparison of CdS films deposited from chemical baths containing different donor type impurities and doping effect to CuInSe$_2$/CdS solar cells", master thesis, supervisor senior research scientist Mare Altosaar.

"Influence of absorber layer chemical treatments on CuInSe$_2$ solar cell parameters", bachelor thesis, supervisor senior research scientist Mare Altosaar.

9. Main areas of scientific work/Current research topics

Natural sciences and engineering; chemistry and chemical technology; new materials and technologies for solar energetics.

List of publications

1) **Ernits, K.**; Muska, K.; Danilson, M.; Raudoja, J.; Varema, T.; Volobujeva, O.; Altosaar, M. (2009). Anion effect of zinc source to chemically deposited ZnS(O,OH) films. Advances in Material Science and Engineering, AMSE/372708.v1 [submitted].

2) **Ernits, K.**; Muska, K.; Kauk, M.; Danilson, M.; Raudoja, J.; Varema, T.; Volobujeva, O.; Altosaar, M. (2009). Chemical bath deposition of ZnS films using different Zn-salts. *In: Physics Procedia: EMRS Spring meeting 2009, Strasbourg, France, 8 - 12 of June 2009.* Elsevier, 2009, BP4-10.

3) **Ernits, K.**; Danilson, M.; Muska, K.; Volobujeva, O.; Altosaar, M. (2009). Chemical Bath Deposited ZnS Thin Films for CuIn(S,Se)$_2$ Solar Cells. *In: Proceedings of 3rd Nordic PV Conference: www.irc.ee/pvconference/download.php?nimi=**ernits**.pdf, 3rd Nordic PV Conference, Tallinn, Estonia, 18-19 May 2009.* , 2009.

4) Hibberd, C. J.; **Ernits, K.**; Kaelin, M.; Mueller, U.; Tiwari, A. N. (2008). Chemical incorporation of copper into indium selenide thin-films for processing of CuInSe$_2$ solar cells. Progress in Photovoltaics: Research and Applications, 16, 585 - 593.

5) Mellikov, E.; Altosaar, M.; Krunks, M.; Krustok, J.; Varema, T.; Volobujeva, O.; Grossberg, M.; Kaupmees, L.; Dedova, T.; Timmo, K.; **Ernits, K.**; Kois, J.; Oja Acik, I.; Danilson, M.; Bereznev, S. (2008). Research in solar cell technologies at Tallinn University of Technology. Thin Solid Films, 516, 7125 - 7134.

6) Hibberd, C. J.; **Ernits, K.** E.; Kaelin, M.; Tiwari, A. N. (2008). Chemical incorporation of copper into indium selenide thin films. 4th Photovoltaic Science, Applications and Technology Conference C89, University of Bath, United Kingdom, 2 - 4 April 2008. , 2008, 052.

7) **Ernits, K.**; Brémaud, D.; Buecheler, S.; Hibberd, C.J.; Kaelin, M.; Khrypunov, G.; Müller, U.; Mellikov, E.; Tiwari, A.N. (2007). Characterisation of Ultrasonically Sprayed InxSy Buffer-Layers for Cu(In,Ga)Se$_2$ Solar Cells. Thin Solid Films, 515, 6051 - 6054.

8) Brémaud, D.; Rudmann, D.; Kaelin, M.; **Ernits, K.**; Bilger, G.; Tiwari, A.N. (2007). Flexible Cu(In,Ga)Se$_2$ on Al-Foils and the effects of Al during Chemical Bath Deposition. Thin Solid Films, 515, 5857 - 5861.

9) **Ernits, K.**; Kaelin, M.; Brémaud, D.; Meyer, T.; Müller, U.; Tiwari, A.N. (2006). Ultrasonically Sprayed In$_2$S$_3$ Films for Cu(In,Ga)Se$_2$ Solar Cells. *In: Proceedings of 21st European Photovoltaic Solar Energy Conference and Exhibition: 21st European Photovoltaic Solar Energy Conference and Exhibition, Dresden, Germany, 4-8 September.* , 2006, 1853 - 1856.

10) Altosaar, M.; **Ernits, K.**; Krustok, J.; Varema, T.; Raudoja, J.; Mellikov, E (2005). Comparison of cds films deposited from chemical baths containing different doping impurities. Thin Solid Films, 480, 147 – 150.

11) Kaelin, M.; Meyer, T.; Meyer, A.; Rudmann, D.; Brémaud, D.; **Ernits, K.**; Tiwari, A.N. (2005). Inorganic TiO2/Cu(In,Ga)Se2 nanocomposit layers for low-cost solar cells. *In: Proceeding of 20th European Photovoltaic Solar Energy Conference and Exhibition: 20th European Photovoltaic Solar Energy Conference, Barcelona, Spain, 6.-10. June.* , 2005, 438 - 441.

12) Kauk, M.; Altosaar, M.; Raudoja, J.; Timmo, K.; Grossberg, M.; Varema, T.; **Ernits, K.** (2005). Tailoring the composition and properties of $CuInSe_2$ materials for solar cell application. Proceedings of SPIE, 224 - 229.

13) Kauk, M.; Altosaar, M.; **Ernits, K.**; Timmo, K.; Jagomägi, A.; Grossberg, M.; Krustok, J.; Varema, T.; Mellikov, E. (2005). Chemical etching of $CuInSe_2$ absorber surface for monograin layer solar cell application. *In: Proceedings of the 20th European Photovoltaic Solar Energy Conference: 20th European Photovoltaic Solar Energy Conference.* , 2005, 1811 - 1815.

Invention

"Method of forming thin film solar cell"; Owner: ETH Zurich; Authors: Ayodhya Nath Tiwari, Kaia Ernits, Chris Hibberd, Marc Kaelin, Maxim Ganchev; Priority number: PCT/CH07/059422; Priority date: 07.09.2007.